Naval Research Laboratory

Washington, DC 20375-5320

NRL/MR/6110--10-9253

Cooling System Design for PEM Fuel Cell Powered Air Vehicles

RICHARD O. STROMAN

Chemical Dynamics and Diagnostics Branch
Chemistry Division

MICHAEL W. SCHUETTE

Global Strategies Group Inc.
Crofton, Maryland

GREGORY S. PAGE

ITT AES
Alexandria, Virginia

June 18, 2010

REPORT DOCUMENTATION PAGE

Form Approved
OMB No. 0704-0188

1. REPORT DATE *(DD-MM-YYYY)*	2. REPORT TYPE	3. DATES COVERED *(From - To)*
18-06-2010	Memorandum Report	January 2007 - December 2009

4. TITLE AND SUBTITLE

Cooling System Design for PEM Fuel Cell Powered Air Vehicles

5a. CONTRACT NUMBER

5b. GRANT NUMBER

5c. PROGRAM ELEMENT NUMBER

6. AUTHOR(S)

Richard O. Stroman, Michael W. Schuette,* and Gregory S. Page†

5d. PROJECT NUMBER

5e. TASK NUMBER

5f. WORK UNIT NUMBER

7. PERFORMING ORGANIZATION NAME(S) AND ADDRESS(ES)

Naval Research Laboratory
4555 Overlook Avenue, SW
Washington, DC 20375-5342

8. PERFORMING ORGANIZATION REPORT NUMBER

NRL/MR/6110--10-9253

9. SPONSORING / MONITORING AGENCY NAME(S) AND ADDRESS(ES)

Office of Naval Research
875 North Randolph Street
Arlington, VA 22203-1995

10. SPONSOR / MONITOR'S ACRONYM(S)

ONR

11. SPONSOR / MONITOR'S REPORT NUMBER(S)

12. DISTRIBUTION / AVAILABILITY STATEMENT

Approved for public release; distribution is unlimited.

13. SUPPLEMENTARY NOTES

*Global Strategies Group (North America) Inc., 2200 Defense Highway, Crofton, MD 21114
†ITT AES, 2560 Huntington Avenue, Alexandria, VA 22303

14. ABSTRACT

The Naval Research Laboratory (NRL) has developed a proton exchange membrane fuel cell (PEMFC) powered unmanned air vehicle (UAV) called the Ion Tiger. The Ion Tiger fuel cell produces 600 W electric (gross) and a comparable amount of waste heat that must be rejected by a cooling system. This study was undertaken to design a cooling system for the Ion Tiger and investigate cooling approaches that may be suitable for future PEMFC powered air vehicles. The performance of several flat plate radiators and compact heat exchangers (CHEs) were evaluated, both in a wind tunnel and in the laboratory. The flat plate radiators were too heavy and occupied too large an area to be practical; a CHE was the lightest and smallest option. A simple thermal model for the flat plate radiators was developed and then used to explain the experimental results. An energy balance model of the fuel cell system and a UA model of the selected CHE were used to size the cooling system. The energy balance and UA models were validated using test flight data. The models were also used to explore the performance envelop of the cooling system which is lightweight, consumes little parasitic power and enables the Ion Tiger to fly continuously at full power in ambient air temperatures up to 55 °C. The combined fuel cell/CHE balance model is applicable (with minor modifications) to other PEMFC systems utilizing a CHE for cooling.

15. SUBJECT TERMS

Unmanned Air Vehicle	PEM	Model	CHE
UAV	Cooling	Thermal	
Fuel cell	Radiator	Compact heat exchanger	

16. SECURITY CLASSIFICATION OF:			17. LIMITATION OF ABSTRACT	18. NUMBER OF PAGES	19a. NAME OF RESPONSIBLE PERSON
a. REPORT	b. ABSTRACT	c. THIS PAGE			Richard O. Stroman
Unclassified	Unclassified	Unclassified	UL	48	19b. TELEPHONE NUMBER *(include area code)* (202) 767-3115

Standard Form 298 (Rev. 8-98)
Prescribed by ANSI Std. Z39.18

Table of Contents

Introduction

The Ion Tiger is an unmanned air vehicle (UAV) under development at the Naval Research Laboratory (NRL) which can remain aloft for 24+ hr carrying a 5 lb, 50 W payload. The proton exchange membrane fuel cell (PEMFC) chosen as the vehicle power system produces waste heat which must be rejected to the environment. The purpose of this study was to understand the available cooling options and choose the one that best balances weight and performance. Included in this report are the evaluation and analysis of several prospective Ion Tiger heat exchangers, the rationale for the final cooling system design, and the predicted/measured system performance.

PEMFCs convert ~55% of the fuel chemical energy to waste heat. Rejecting that heat can be challenging due to the low (60 – 70 °C) PEMFC operating temperature; in a hot environment (40 °C) the small temperature difference between the radiator and ambient air leaves little gradient with which to reject the heat. The small temperature gradient dictates a large heat transfer area, but air vehicles have stringent weight restrictions so care must be taken to choose the lightest cooling option.

The study had six parts: (1) measuring the heat transfer characteristics of several radiators, (2) using the measurements to create radiator models, (3) creating a fuel cell energy balance model to predict the required rate of heat rejection, (4) selecting a radiator based on the heat rejection prediction and radiator models, (5) coupling the radiator and fuel cell models for a design sensitivity analysis and (6) validating the models with flight data.

Two radiator types were evaluated; surface radiators and compact heat exchangers (CHEs)[*]. The surface radiators were designed to be mounted on the outside of the fuselage where vehicle motion would drive air over them. One CHE was also designed for mounting on the outside of the fuselage. The remaining CHEs were designed to be mounted inside the fuselage with air ducted through them. Airflow through the internal radiators would be driven by a combination of vehicle motion and a fan. The surface radiator concept was motivated by its low aerodynamic drag, whereas the CHE concept was motivated by the high efficiency and durability of "tube and fin" style CHEs. Four surface radiators and one CHE were evaluated in a wind tunnel to replicate conditions on the surface of the Ion Tiger fuselage. Four CHEs were evaluated using an apparatus that simulated the airflow from a duct and fan.

The surface radiator models relied on a flat plate Nusselt number correlation to predict the total heat rejection given the inlet coolant temperature, air temperature and air speed. The same inputs were used with simple log mean temperature difference (LMTD) models to predict the total heat rejection from CHEs. The required rate of heat rejection was predicted by a fuel cell energy balance model. The energy balance model accounted for the rate of water condensation in the stack, a key contributor to the rate of waste heat production. The radiator and stack models were coupled to find the size and weight of radiator required to cool the Ion Tiger under worst-case conditions at steady state, and to carry out a design sensitivity analysis.

The Ion Tiger must operate with a gross fuel cell stack electrical output of 600 W in ambient air temperatures of at least 38 °C. This and other specifications important to the cooling system are listed in Table I. Some items in Table I are limitations imposed by the fuel cell, fuel cell balance of plant or aircraft design. For example, the coolant pump supplies a maximum 2 L/min with 1 psi pressure drop across the radiator, so the radiator design must accommodate this limit.

TABLE I. Ion Tiger cooling system design parameters.

Parameter	Value
Maximum coolant water flowrate	2.0 L/min
Maximum air velocity through an internal radiator	100 sft^3/min
Air flow velocity over a surface radiator (cruise airspeed)	27 knots
Maximum coolant temperature at the radiator outlet	70 °C
Minimum typical coolant temperature at the fuel cell inlet	55 °C
Minimum ambient air temperature	38 °C
Maximum coolant side pressure drop	1 lb/in^2
Maximum radiator mass (including coolant)	680 g
Gross fuel cell electrical output @ cruise	330 W_e
Gross fuel cell electrical output @ full power	600 W_e
Stack voltage @ full power	21 V (0.58 V/cell)
Current @ min voltage and full power	29 A

[*] In this report the terms compact heat exchanger and surface radiator are only used when the distinction is important; in most cases they are both referred to simply as radiators.

Manuscript approved January 27, 2010.

Radiator Measurements

The primary goal was to measure the overall heat transfer coefficient, U_{rad}, of each radiator, i.e. the heat transfer rate per unit area of radiator per degree difference between the ambient air temperature and average radiator temperature. Note that this is a gross heat rejection metric for the whole radiator, not the local heat transfer coefficient, h. All measurements were carried out at steady state to ignore the effects of the coolant and radiator heat capacities on transients. Secondary goals were to measure the coolant and air side pressure drops through each radiator.

Radiators Considered

Surface Radiators

Each surface radiator consisted of a 12 x 18 inch rectangular G-10 fiberglass panel, ½ inch thick, with V-shaped grooves cut in the surface to act as flow channels. The grooves had the profile of an equilateral triangle with side length 0.350 inch, except for a 0.095 inch fillet at the bottom of the groove. A sheet of 0.005 inch thick aluminum alloy 1100 was adhered to the surface of the panels to close the grooves and form channels. The double sided adhesive tape used to bond the aluminum to the panels was 0.020 inch thick 4905 VHB DC Acrylic Foam. Once closed, the grooves became channels with a hydraulic diameter of 3/16 inch. The inlet and outlet for each channel were brass barb fittings threaded into tapped holes in the back of the G-10 plate. Aluminum was chosen to close the channels because it provides a high thermal conductivity path from the water to air, and because it was expected to increase the area for convective heat transport by conducting some heat laterally. The groove and sheet construction technique was chosen because the air vehicle engineers believed they could create a similar structure in the fuselage of the Ion Tiger. This was expected to reduce the radiator weight by being multifunctional; the radiator would serve both structural and thermal purposes. The configurations of each surface radiator are listed in Table II.

TABLE II. Characteristics of the four flat surface radiators evaluated in the wind tunnel. Total aluminum surface area for each of the radiators was 1394 cm^2.

Name	Geometry	Number of Channels	Number of Passes/channel	Total Water-Al-Air Wetted Area [cm^2]	Fraction of Wetted Area in Counter/Co-Flow
Radiator #1	Serpentine, Widely Spaced	1	4	218	.5/.5
Radiator #2	Serpentine, Closely Spaced	1	6	266	.5/.5
Radiator #3	Parallel, Widely Spaced	10	1	359	1/0
Radiator #4	Parallel, Closely Spaced	20	1	568	1/0

Radiators #1 and #2 had a single serpentine channel with an even number of passes. They were oriented with respect to the air flow such that half of the total channel length was in counter flow and the other half was in a parallel flow configuration. The inlet and outlet were on opposite corners of the plate at each end of the channel. Radiators #3 and #4 had multiple channels oriented in a counter flow configuration, all of which were connected in parallel to manifolds at opposite ends of the plate. The inlet and outlet were on opposite corners of the plate, one feeding each manifold. Flat radiators with serpentine and parallel channels are illustrated in figure 1.

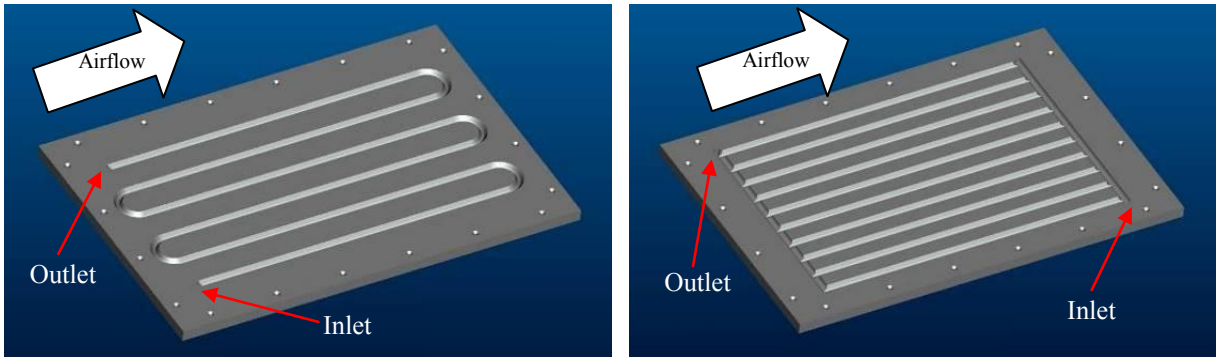

Figure 1. Pro/Engineer models of radiators #2 (left) and #3 (right) before installation of the aluminum sheet.

Compact Heat Exchangers

Radiator #5 was the one CHE designed to be mounted on the outside of the aircraft fuselage. It was fabricated by AeroVironment for a 250 W PEMFC powered UAV. This radiator consisted of a single coolant flow channel with fins

attached via dip-brazing. The fins were a continuous strip of bent aluminum with every other bend in contact with the coolant channel. Bent fins were straightened before testing, but some irregular spacing remained. There were 100 fins total, each of which was 1.0 inches long in the direction of airflow, 1.2 inches high and spaced approximately 0.0475 inches apart. The air flow cross-section of the radiator used to calculate the heat transfer coefficient had an area of 36.7 cm^2. Figure 2 is a photograph of radiator #5 from a perspective in which the direction of air flow would be into or out of the page.

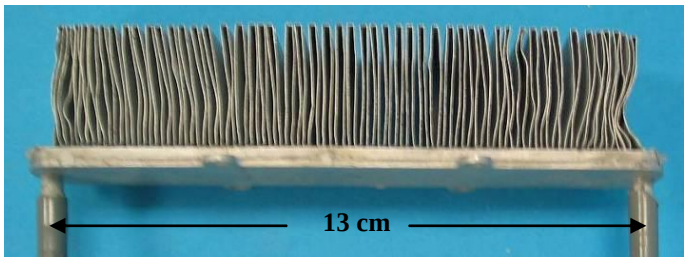

Figure 2. Radiator #5.

Radiator #6 was fabricated by NRL using a 14 × 11.5 × 3 cm block of interconnected aluminum cells (aluminum foam). The cell diameters ranged from 3 – 10 mm (see figure 3). 16 passes of 1/8 inch O.D. aluminum tubing in series passed through the foam to carry coolant. The passes were divided evenly into two planar banks perpendicular to the direction of airflow, one plane ahead of the other. Coolant flowed through the rear bank of tubes first, then through the forward bank so that the radiator was in a semi-counter flow configuration. Air flowed only through the foam section in testing, not over the tube loops protruding from the ends of the foam.

The fabrication of radiator #6 began with the aluminum foam, which is a commercial product. The tubing was bent with lead solder inside to prevent it from collapsing. Once bent, the two layers of tubing were sandwiched between three thin layers of aluminum foam. The sandwich was compressed until the broken cell walls at the surface of each foam layer interlocked. This made the foam behave as a monolithic block and brought it into intimate physical (and thermal) contact with the tubes. The structure was given additional strength by applying an adhesive (JB Weld) where the tubes emerge from the foam. In figure 3 two power resistors are shown attached to radiator #6, but they played no role in the heat transfer measurements.

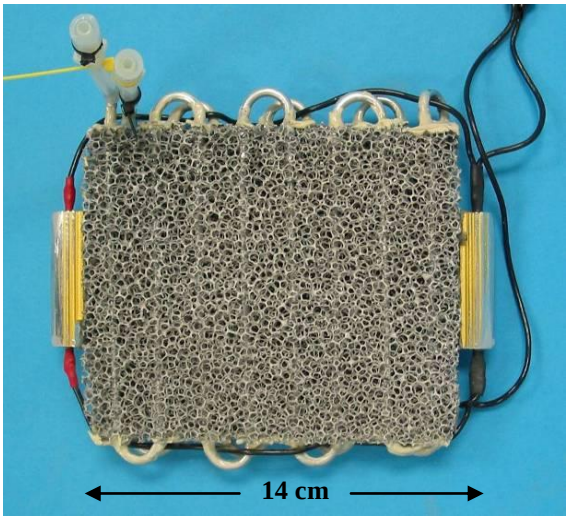

Figure 3. Radiator #6

Radiator #7 was assembled at NRL using a custom (purchased) radiator core. The tanks and ports were fabricated at NRL, and then the whole assembly was welded together. The core construction consisted of narrow tubes with louvered fins between them. A custom fan and shroud were designed and built by NRL for radiator #7. The fan blades and shroud were formed using stereo lithography; the fan motor was a brushless DC motor with motor controller. These fan and shroud designs were chosen because the structure was lightweight and because the motor was very efficient. Figure 4 shows a photograph of radiator #7.

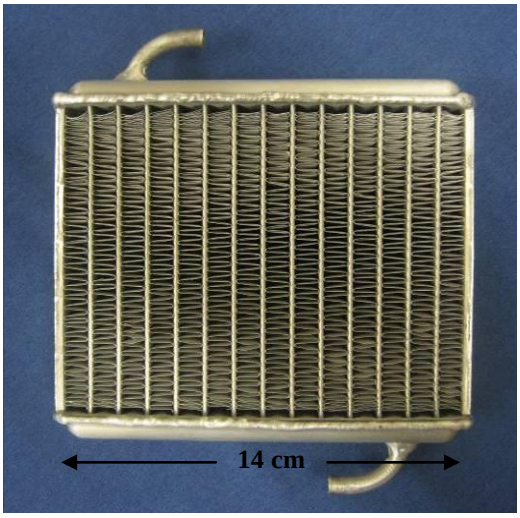

Figure 4. Radiator #7.

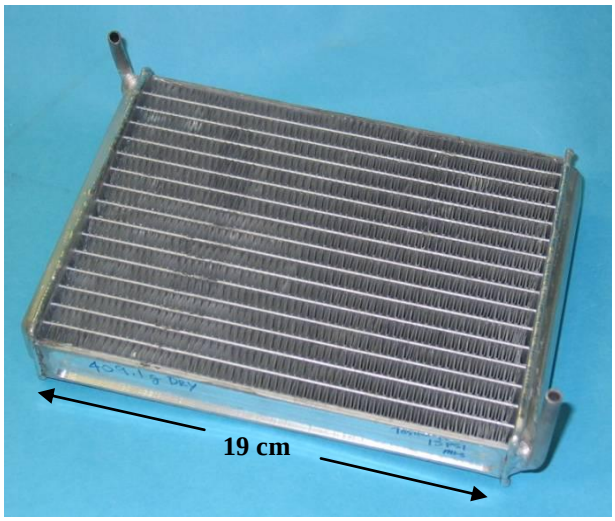

Figure 5. Radiator #8.

Radiator #8 was also assembled at NRL and had the same design as radiator #7; the only differences were that it had roughly twice the air flow area and two fans. There were two reasons for measuring the heat transfer characteristics of such similar radiators. First, the heat transfer coefficient is normalized to area, so including two radiators of the same design but different areas is a good check on the experimental method. Second, there were two PEMFC powered UAV programs in progress at NRL the time of this study. Radiators #7 and #8 were sized based on rough estimates of radiator performance and the amount of heat each UAV would need to reject. Radiator #8 (shown in figure 5) was intended for use in the Ion Tiger. Figure 6 is a photograph of radiators #7 and #8 with their shroud and fan assemblies. The small cylinder to the left in figure 6 is a tank used to remove air bubbles from the coolant loop. The fan shrouds and de-bubbler tank were designed at NRL and fabricated using a sterolithographic process.

Figure 6. Radiators #7 (left) with the custom fan assembly and radiator #8 (right) with just the fan shroud. Also in the photograph are a tank for removing air from the coolant (white cylinder) and one of the custom stamped end tanks welded to the radiator cores at NRL.

Radiator #9 was a commercial off the shelf (COTS) motorcycle radiator with a core design similar to that of radiators #7 and #8. One problem encountered when designing the Ion Tiger cooling system was that most COTS radiators were designed for much higher air and coolant flowrates than were expected in the Ion Tiger. This radiator was included in the study as an example of the existing lightweight COTS radiator technology. Since radiator #9 was designed to cool an internal combustion engine, it was not clear before testing how well it would perform in this application. Radiator #9 was made of aluminum and had louvered fins to raise the rate of heat transfer by disturbing the air thermal boundary layer. Coolant inlet and exit ports were added at NRL so that they would be compatible with barb fittings and the silicone coolant transfer lines

used in this study. Figure 7 is a photograph of radiator #9 from a perspective in which the direction of air flow would be into or out of the page.

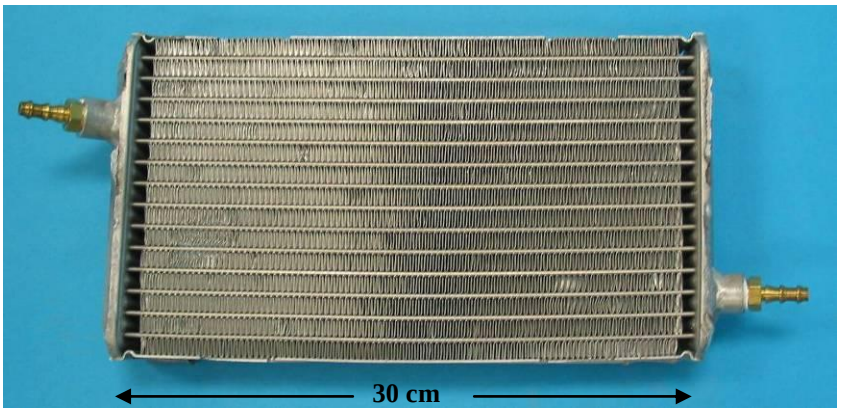

Figure 7. Radiator #9

Table III summarizes the physical characteristics of all five CHEs evaluated. The last column in Table III lists the radiator mass (when filled with water, including tanks) divided by the area through which air flows. Normalizing the mass in this way was useful when comparing the heat transfer performance of multiple radiators because the overall heat transfer coefficient is also normalized to the radiator air flow area.

TABLE III. Characteristics of the compact heat exchangers.

Name	Channels	Passes per channel	Cross Section Area ⊥ to Airflow [cm^2]	Fin Length, Depth [cm]	Fin Spacing [mm]	Dry Mass [g]	Wet Mass [g]	Mass/Air Flow Area [g/cm^2]
Radiator #5	1	1	37	3.0, 2.5	1.2	70	76.6	2.08
Radiator #6	1	16	161	NA	NA	155	170	1.06
Radiator #7	13	1	134	0.8, 2.4	1.0	225	309	2.31
Radiator #8	15	1	304	0.8, 2.4	1.0	409	600	1.97
Radiator #9	14	1	362	0.8, 2.4	1.0	504	670	1.85

Measurement Setup

Water was heated to approximately 65 °C in a thermal bath and then pumped through 1/4 inch I.D. polyethylene tubing to each radiator at a rate between 0.75 and 2.0 L/min. The water flow rate, temperature at the radiator inlet and temperature at the radiator outlet were measured; from these measurements the rate of heat rejection could be calculated. A pressure transducer was used to measure the difference in water pressure between the radiator inlet and outlet. Figure 8 shows a schematic of the measurement setup; for the details of each component refer to Table IV.

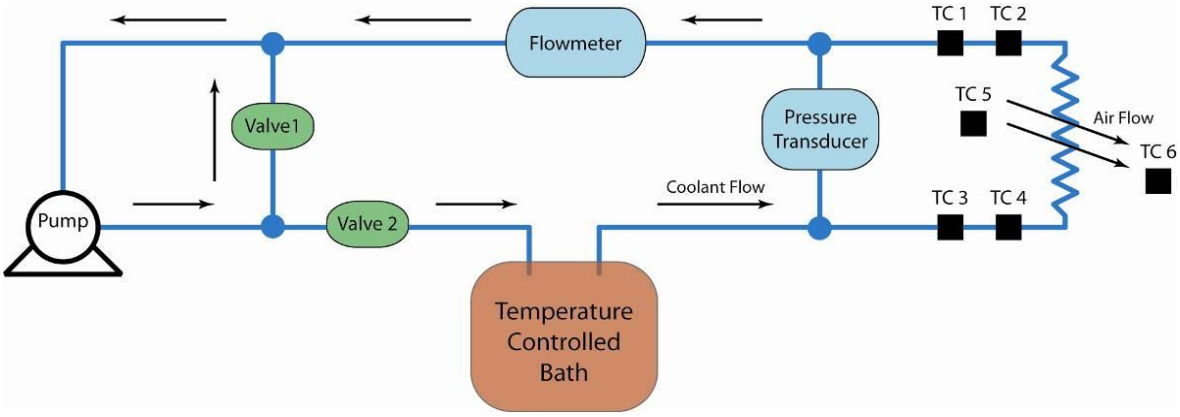

Figure 8. Schematic of the measurement setup in which thermocouples are indicated by "TC" and blue lines are water flow paths.

TABLE IV. Equipment used in radiator measurements.

Equipment	Manufacturer/Part Number	Range	Accuracy
Water flow meter	McMillan Co./S111	0.5 – 2 L/min	± 3% full-scale
Pressure Transducer	Cole-Parmer/68071-58	0 – 10 lb/in^2	± 0.25% full-scale
Thermocouples	Omega/K-type	-100 – 1300°C	N/A
Water Thermocouple Reader	Omega/HH147	-100 – 1300 °C (K-type)	± (0.1% rdg + 0.7 °C)
Air Thermocouple Reader	Omega/HH303	-100 – 599 °C (K-type)	± (0.1% rdg + 0.7 °C)
Anemometer	Omega/HHF802	0.4 – 25 m/s	0.1 m/s res, ± (2% rgd + 1 digit)
Temperature Bath	VWR/116OS	-20 – 150 °C	± 0.5 °C
DAQ Board	National Instruments/6024E	-10 – 10 V	
Water Pump and Pump Motor	Baldor		N/A
Fan(s)	Mechatronics/F1238X-H	0 – 130 ft^3/min 0.37 – 0 in H_2O	N/A

Water was pumped in a loop at a nearly constant flow rate with a fraction of the flow diverted through the radiator. The flow fraction through the radiator was set by adjusting two valves. In some cases the temperature controlled bath was unable to supply enough heat to raise the water returning from the radiator to 65 °C, so it was augmented by a 1 kW resistive heater immersed in the bath. The differential pressure transducer was connected to the radiator inlet and outlet via silicone tubing and barbed polyethylene "T" fittings. The silicone tubing was secured on the "T" fittings by wrapping the junctions with cable ties. The differential pressure transducer produced a 4 – 20 mA current signal proportional to the pressure difference which was read by passing it through a 980 Ω resistor, measuring the voltage across the resistor and applying Ohm's Law (see equation 1). The voltage was read and recorded using a data acquisition (DAQ) board and computer code written in LabView. Figure 9 shows a schematic of the circuit used to read the pressure transducer output.

$$I_{signal} = \frac{V_{resistor}}{R_{resistor}} \quad [1]$$

The pressure transducer was calibrated by exposing the high side pressure tap to columns of water of various known heights, calculating the pressure from each column, and comparing to the transducer output. Equation 2 gives the pressure P exerted by a column of water of density ρ and height y in a gravitational field of strength g. The transducer response was linear with m = 0.63 psi/mA. The LabView code calculated pressure from the transducer current using equation 3.

$$P = \rho g y \quad [2]$$

$$P = m I_{signal} \quad [3]$$

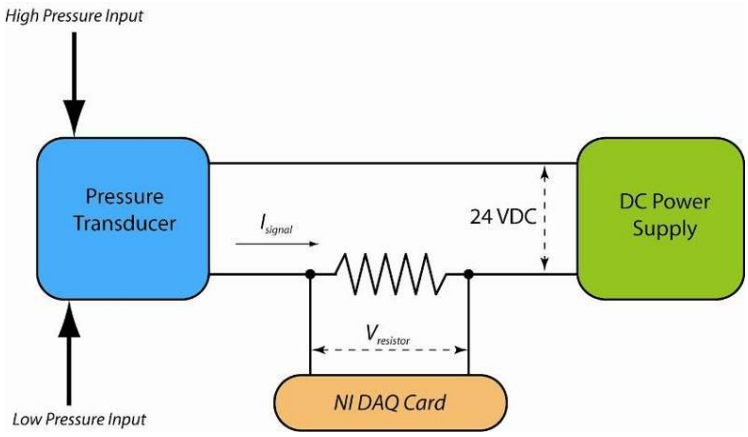

Figure 9. Schematic of the pressure transducer circuit.

A turbine-style flow meter was used to measure the water flow rate. The flow meter produced a voltage signal proportional to the flow rate which was read and recorded by the same DAQ card reading the pressure transducer signal. The flow meter also had a built-in display, which simplified the processes of adjusting the flow rate.

Small changes in temperature corresponded to large changes in the rate of heat transfer from the radiator due to the large specific heat of water. To mitigate the effect of random error on the water temperature measurements, the average from two thermocouples was used at both the radiator inlet and outlet. The four thermocouples were potted in polyethylene T-fittings spliced into the water transfer lines to ensure good thermal contact. They were calibrated in an ice/water bath and in boiling water. The same thermocouple reader was used for all water temperature measurements. It was unnecessary to average measurements over time because the water temperature fluctuated little.

Only one thermocouple was used for each air temperature measurement because the heat capacity of air is so low that small errors had relatively little impact on the calculated heat transfer rate. The same thermocouple reader was used for the inlet and (in the cases where it was measured) the outlet air temperature measurements. Once the system had reached steady state, air temperature measurements were logged at 1 s intervals and then averaged over 180 s to arrive at the measured value.

The NRL wind tunnel was built by FluiDyne Engineering (Minneapolis, MN) and features a 4 ft by 4 ft by 7 ft long test section and a speed range of 20 to 200 knots. The temperature of air entering the test section is measured by a thermistor in the stilling chamber and reported at the control station. While the test section is indoors, most of the tunnel is outdoors, so the temperature and humidity of air in the tunnel vary with the changes in the outdoor environment. Windows in the test section allow users to view the experiment.

Setup for Measurement #1

A boundary layer plate was installed in the wind tunnel to simulate the outside surface of the Ion Tiger fuselage. The plate was oriented horizontally (parallel to airflow direction) and located in the center of the tunnel width-wise and 1/3 of the wind tunnel height from the floor to minimize wall effects. The plate leading edge was tapered to produce a "clean" boundary layer relatively free of disturbances. See figure 10 for a photograph of the boundary layer plate installed in the wind tunnel. Radiators #1 through #4 were set flush in the boundary layer plate 15 inches from the leading edge to approximate the Reynolds number they would experience if installed on the outside of the Ion Tiger fuselage.

A boundary layer rake with 12 pitot tubes (see figure 11 for an illustration) was installed on the boundary layer plate behind the surface radiators to profile the momentum boundary layer and assess the transition to and magnitude of turbulent flow. A reference pitot tube was installed ahead of the radiator. The pressures experienced by the pitot tubes were measured by a manometer containing colored methanol. Methanol was chosen for its low density (0.7918 g/cm^3 at 20 °C and 1 ATM) which provided better resolution than water. Various height "trips" were added to the boundary layer plate ahead of the radiators to induce air turbulence and raise the rate of heat transfer.

Silicone rubber tubing was used to transfer heated water between the radiator and the thermal bath outside the wind tunnel. Fiberglas insulation was wrapped around the tubing to reduce the amount of heat required from the bath, but since coolant temperature was measured at the radiator inlet and outlet, heat lost from the tubing did not affect accuracy. The inlet air temperature was measured both by a thermocouple installed in the wind tunnel, and by one installed on the boundary layer plate ahead of the radiator. An attempt was made to measure the air outlet temperature, but the air temperature varied so much with position that a reliable measurement could not be made.

The wind tunnel air speed was 27 knots, the predicted cruise speed of the Ion Tiger. The wind tunnel air (radiator inlet air) temperature was uncontrolled and therefore varied among the measurements depending on the weather. This variation should not have affected the results significantly because the heat transfer coefficient was normalized to the temperature difference between the water and air.

The rate of convective heat transfer from a plate is substantially greater when the airflow over it is turbulent rather than laminar. Pin striping tape was adhered to the boundary layer plate ahead of the radiator to form a trip and induce turbulent flow. The overall heat transfer coefficients of two surface radiators were measured with several different trip heights (up to a limit, greater trip height translates roughly into greater turbulence) to evaluate the utility of a trip on the Ion Tiger.

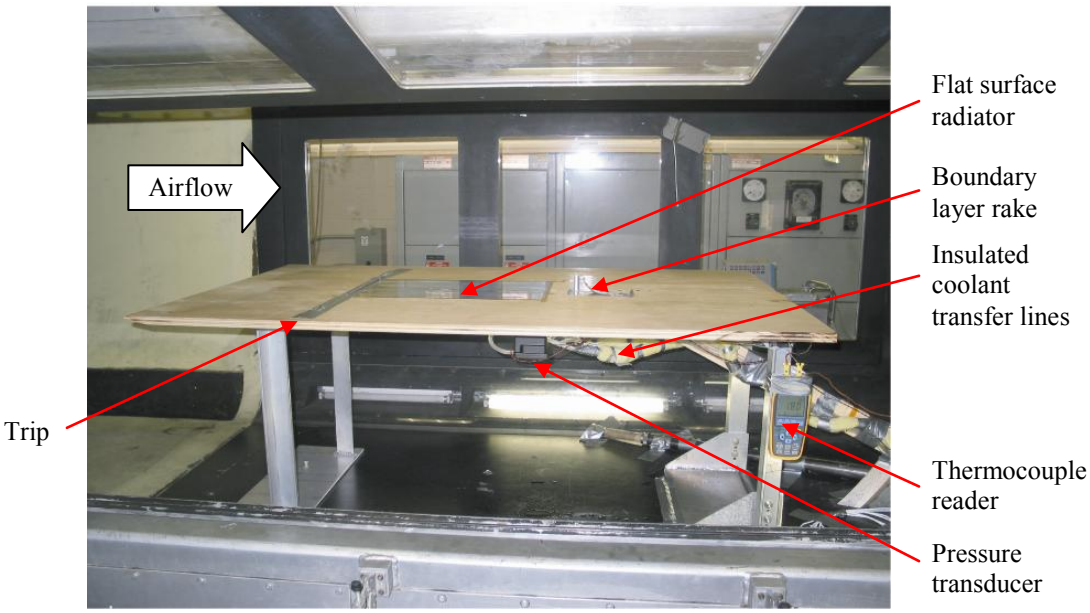

Figure 10. Boundary layer plate installed in the wind tunnel for measurement #1.

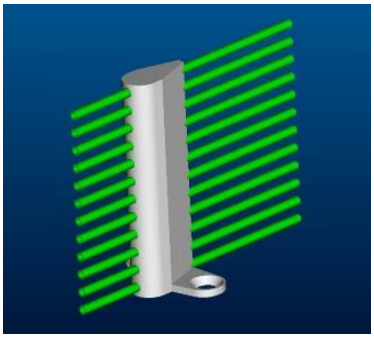

Figure 11. Pro/Engineer model of boundary layer rake used for measurement #1.

Setup for Measurement #2

The setup for Measurement #2 was the same as for Measurement #1 except that the surface radiator was replaced by radiator #5. A blank G-10 panel with radiator #5 attached to it was set in the boundary layer plate in place of a surface radiator. Radiator #5 was located near the front edge of the G-10 plate so it would experience the same Reynolds number as the surface radiators. It was oriented so that the air flow would be parallel to the fins, i.e. blow between them. The water inlet and outlet ran through holes in the G-10 plate and had the silicone tubing to/from the thermal bath clamped to them with cable ties.

Setup for Measurement #3

The same water loop used in Measurements #1 and #2 was used in Measurement #3. Instead of the wind tunnel, a different apparatus was used to measure the overall heat transfer coefficients of radiators #6-#8. The apparatus made it possible to measure the air inlet temperature, air outlet temperature and air flow rate in addition to the water flow rate and temperature. The apparatus consisted of two chambers; ambient air was drawn through a radiator set in the surface of the first chamber and exhausted through an anemometer set in the surface of the second chamber. A fan was placed between the chambers to drive the air flow. This arrangement was chosen because it ensured that air exiting the radiator was well mixed for the temperature measurement and because it allowed extraneous air currents from the fan to dissipate before passing through the anemometer.

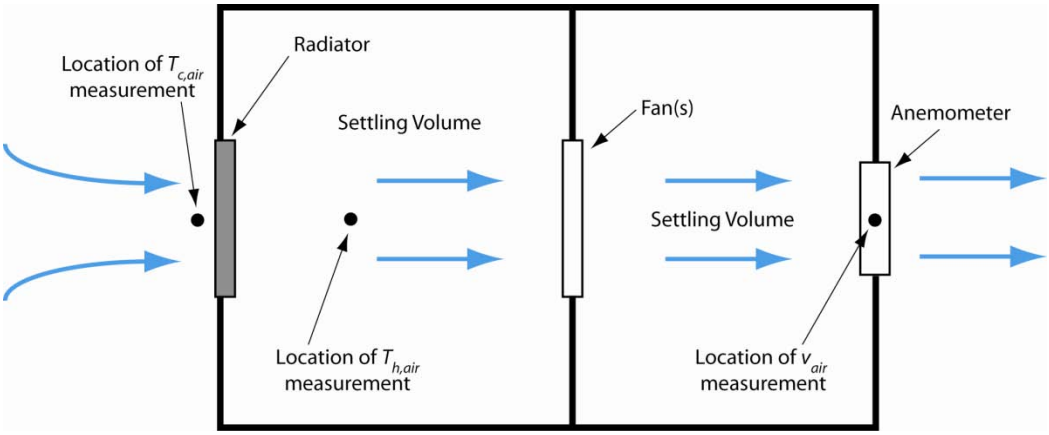

Figure 12. Bench top apparatus for Measurements #3 and #4.

The volumetric air flow rate was computed by multiplying the air speed from the anemometer by the area of its orifice. The anemometer had a built in thermocouple, so it reported the temperature of the air flowing through it. This air temperature was used to compute the air density and air mass flow rate.

Once the air flow rate was known, it was possible to estimate the static air pressure drop across the radiators by referring to the fan manufacturer's pressure-flow rate curve (figure 13). This was only an estimate because the anemometer imposed an additional flow restriction, so the actual air pressure drop across the radiator was lower than the value indicated by figure 13. This translated to a slight overestimate of the airflow rate, but such an error only makes the final design more conservative.

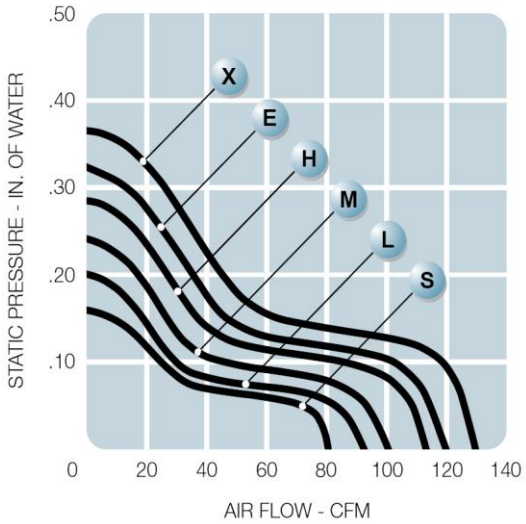

Figure 13. Flow rate – pressure curves generated for each fan available from the manufacturer (Mechatronics, Inc.). The fan corresponding to curve X was used in these measurements.

Setup for Measurement #4

Measurement #4 was intended not only to measure the heat transfer characteristics of radiator #9, but also to compare the wind tunnel and bench top measurement methods. Radiator #9 was run in the wind tunnel with largely the same setup as in Measurement #2, and then it was run in the apparatus with the same setup as in Measurement #3.

Setup for Measurement #5

For Measurement #5 each radiator was installed in the coolant flow loop, then the water side pressure drop was measured at 1.0, 1.25, 1.5, 1.75 and 2.0 L/min. The only exception was radiator #5 for which the range had to be reduced because the pressure drop was so large at higher flow rates that the silicone tubing failed. The water temperature for these measurements was approximately 60 °C, so the viscosity and pressure drop were similar to those expected in the Ion Tiger.

Data Reduction Methods

Energy conservation dictates that the rate of heat rejection by a radiator at steady state is equal to the change in enthalpy of the hot fluid flowing through it. The rate of heat rejection by each radiator was computed using equation 4, which assumes the density and specific heat of the fluid are constant and defined at the average fluid temperature. The variables in this section are listed and defined in Table V.

$$\dot{Q}_{rad} = \dot{m}_{coolant}\left(i_{in} - i_{out}\right) = \rho_{coolant}\dot{V}_{coolant}c_{p,coolant}\left(T_{coolant,in} - T_{coolant,out}\right) \quad [4]$$

The overall heat transfer coefficient of each radiator was calculated using Newton's Law of Cooling (equation 5).

$$U_{rad} = \frac{\dot{Q}_{rad}}{A_{norm}\Delta T_{air-coolant}} \quad [5]$$

The overall heat transfer coefficients for radiators #1 through #4 were normalized to the radiator surface parallel to the direction of airflow. The overall heat transfer coefficients for radiators #5 through #9 were normalized to the radiator area perpendicular to the direction of airflow. The normalization areas are illustrated in figure 14.

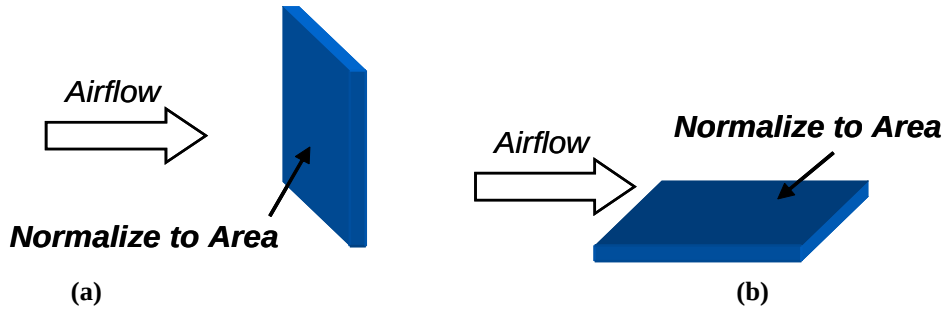

Figure 14. Areas used to compute the overall heat transfer coefficients of (a) radiators #1 through #4 and (b) radiators #5 through #9.

TABLE V. Variables involved in calculating radiator measurement results.

Variable	Meaning	Unit
$\dot{Q}_{rad}$	Rate of heat rejection from the radiator	W
$\dot{m}_{coolant}$	Mass flow rate of coolant through the radiator	kg/s
$\rho_{coolant}$	Density of coolant	kg/m^3
$\dot{V}_{coolant}$	Volumetric flowrate of coolant	m^3/s
$c_{p,coolant}$	Specific heat of the coolant (in this case c_p = 4183 J/(kg °C) at 60 °C)	J/(kg °C)
$T_{coolant,in}$	Temperature of coolant entering the radiator	°C
$T_{coolant,out}$	Temperature of coolant exiting the radiator	°C
$T_{air,in}$	Temperature of air entering the radiator	°C
$T_{air,out}$	Temperature of air exiting the radiator	°C
$\Delta T_{air-coolant}$	Mean temperature difference between the air and radiator	°C
A_{norm}	Area to which the heat transfer coefficient is normalized	m^2
U_{rad}	Overall heat transfer coefficient of the radiator	W/(m^2 °C)
A_{air}	Area of the aperture through which air is flowing when its velocity is measured.	m^2

Two different methods were used to determine the mean air-water temperature difference $\Delta T_{air-coolant}$ used in equation 5. For Measurements #1 and #2 the value of $\Delta T_{air-coolant}$ was determined using equations 6 and 7 because the heat transfer rates were small, turbulence made the change in air temperature small, and the outlet air temperature was not measured reliably.

$$T_{coolant,av} = \tfrac{1}{2}\left(T_{coolant,in} + T_{coolant,out}\right) \quad [6]$$

$$\Delta T_{air-coolant} = T_{coolant,av} - T_{air,in} \quad [7]$$

To process most of the data from Measurements #3 and #4 the log mean temperature difference (LMTD) for a counter flow heat exchanger was used. The LMTD accounts for the different rates at which the hot and cold fluid temperatures change as they flow through the heat exchanger (see equation 8), so in some cases it is far more accurate than the arithmetic mean. The LMTD is preferable to the arithmetic mean when $r > 1.5$ in equation 9. The correction factor F in equation 8 accounts for the geometry in compact heat exchangers, and is determined using figure 15 in conjunction with R and P in equations 10 and 11.

$$\Delta T_{air-coolant} = F\,\frac{\left(T_{coolant,in} - T_{air,out}\right) - \left(T_{coolant,out} - T_{air,in}\right)}{\ln\left(\dfrac{T_{coolant,in} - T_{air,out}}{T_{coolant,out} - T_{air,in}}\right)} \quad [8]$$

$$r = \frac{T_{coolant,in} - T_{air,in}}{T_{coolant,out} - T_{air,out}} \quad [9]$$

$$R = \frac{T_{coolant,in} - T_{coolant,out}}{T_{air,out} - T_{air,in}} \qquad P = \frac{T_{air,out} - T_{air,in}}{T_{coolant,in} - T_{air,in}} \quad [10, 11]$$

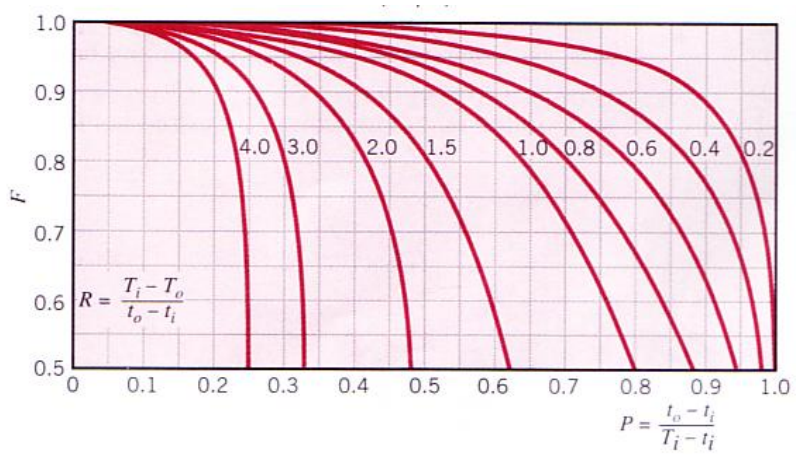

Figure 15. Correction factor for a single-pass, cross-flow heat exchanger with both fluids unmixed. [3]

If one assumes heat is only lost to the cold fluid and the radiator is at steady state, then conservation of energy can be applied to the air side energy balance. The air side data from Measurements #3 and #4 was checked this way against the water-side heat transfer rate using equation 12. Equation 12 is simply equation 4 rewritten for the air side, where the volumetric flow rate of air is expressed as the product of air velocity v_{air} and orifice area A_{air} (see equation 13). The air density, velocity and specific heat were evaluated at the air outlet temperature $T_{air,out}$.

$$\dot{Q}_{rad} = \dot{m}_{air} c_{p,air}\left(T_{h,air} - T_{c,air}\right) = \rho_{air}\dot{V}_{air} c_{p,air}\left(T_{h,air} - T_{c,air}\right) \quad [12]$$

$$\dot{V}_{air} = v_{air} A_{orafice} \quad [13]$$

Measurement Results

Results from Measurement #1

The measured overall heat transfer coefficients for radiators #1 through #4 without a trip are listed in Table VI. The values in Table VI are averages over different water flow rates (~0.5, ~1.0 and ~1.5 L/min) and inlet water temperatures (50 °C and 70 °C). Variations in coolant flow rate and inlet temperature were shown to have little influence on the heat transfer coefficient, which was expected over the ranges examined in this study (see figures 16 and 17).

Table VI includes heat transfer coefficients normalized to the total aluminum sheet area and to the wetted aluminum area. These are lower and upper bounds on the actual value which depends on the amount of lateral heat conduction by the aluminum sheet. If the aluminum sheet is a perfect conductor then the heat transfer coefficient should be normalized to the entire sheet area. If the aluminum sheet does not conduct any heat laterally, then the heat transfer coefficient should be normalized to the wetted aluminum area. The modeling described in later sections shed light on where in this range the true values fell.

TABLE VI. Overall heat transfer coefficients for radiators #1 through #4 measured in the wind tunnel with no trip and a free stream airspeed of 27 knots. Each value is an average of steady-state measurements at water inlet temperatures of 50 °C and 75 °C, and water flow rates of 0.5, 1.0 and 1.5 L/min.

Name	U_{rad} [W/(m^2 °C)] normalized to total Al area	U_{rad} [W/(m^2 °C)] normalized to wetted Al area
Radiator #1	38	241
Radiator #2	46	243
Radiator #3	50	194
Radiator #4	46	113

Two methods were employed to assess the extent of heat transfer laterally in the aluminum sheet, but neither was successful. A thermal camera was used to image the flat plate radiator, but the temperature difference between the ambient air and the radiator was smaller than the minimum temperature difference detectable by the camera. A thermal camera with greater sensitivity would likely have worked. A thermocouple was placed in contact with various points on the radiator surface, but the measurement was corrupted by heat transfer from the thermocouple to the air flowing over the radiator.

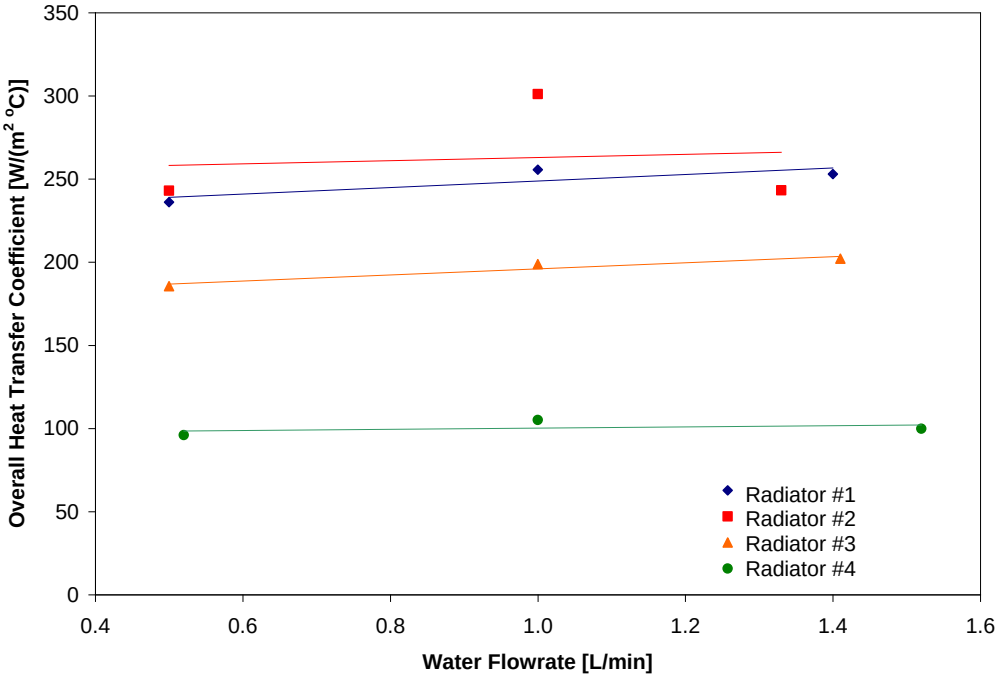

Figure 16. Plot showing that the heat transfer coefficient for radiators #1 through #4 had little dependence on water flow rate (between 0.4 and 1.4 L/min). In this figure the heat transfer coefficient is normalized to the air-water wetted area of the channels. The water inlet temperature was 50 °C for these measurements. Lines on the plot are only aids to the eye in seeing trends.

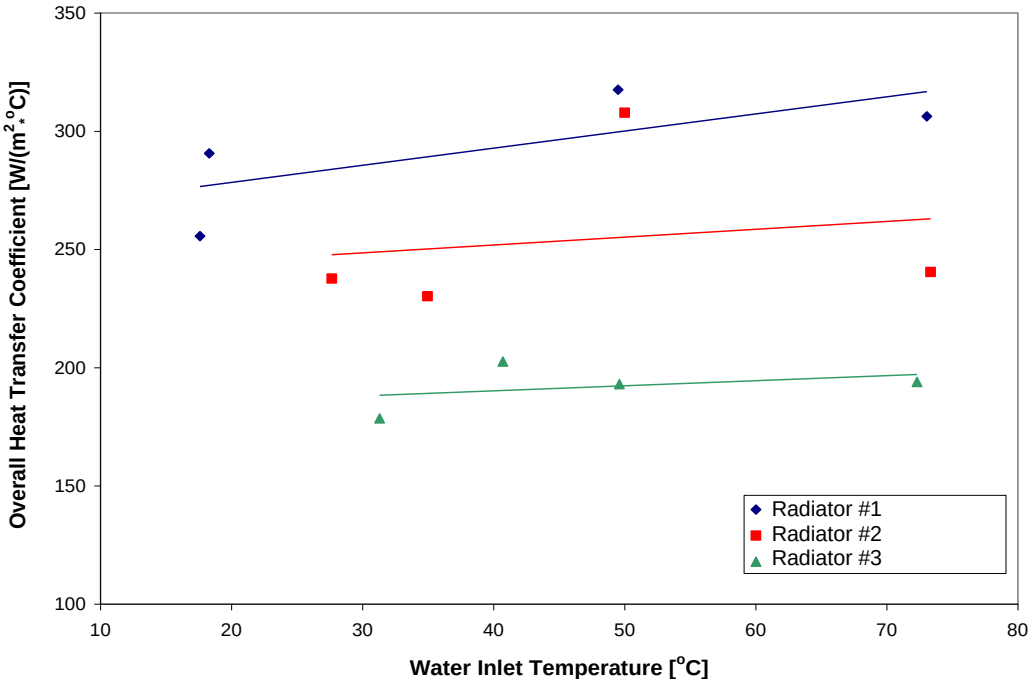

Figure 17. Plot showing that the heat transfer coefficient for radiators #1 through #4 had little dependence on coolant inlet temperature (between 25 - 75 °C). In this figure the heat transfer coefficient was normalized to the air-water wetted area of the channels. The water flow rate was 1.0 L/min for these measurements. Lines on the plot are only aids to the eye in seeing trends.

Figure 18 shows that trip height had little influence on the overall heat transfer coefficient, which suggests that the air flowing over the radiator was already turbulent without a trip. This conclusion was confirmed by measurements using the boundary layer rake, which indicated that a turbulent boundary layer had formed before the addition of a trip. Based on this measurement, trips ahead of a surface radiator on the Ion Tiger would increase aerodynamic drag without improving radiator performance.

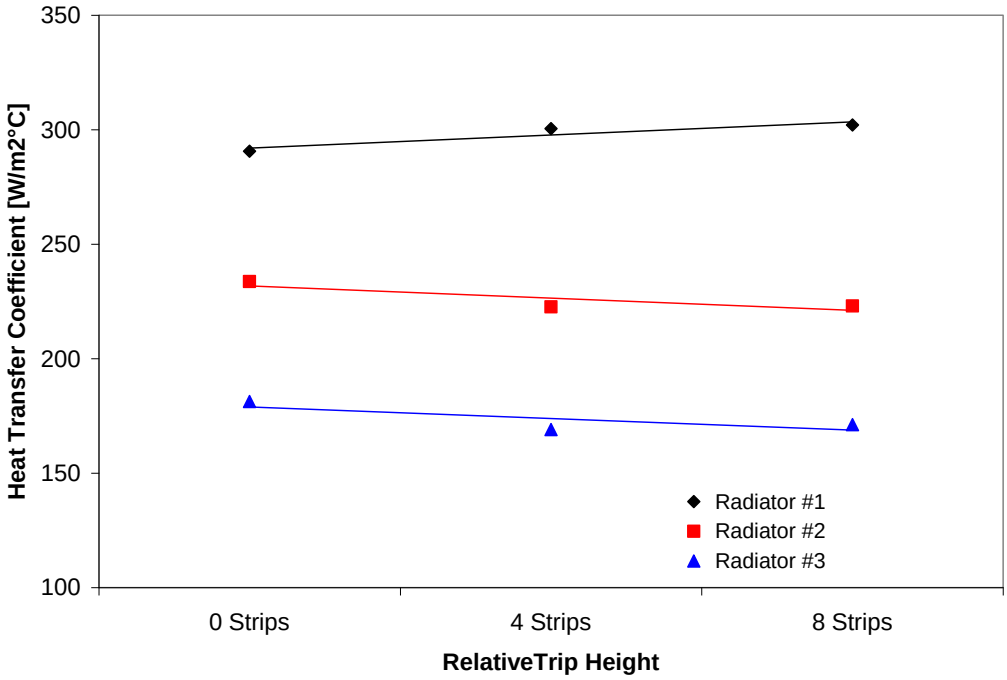

Figure 18. Plot showing the lack of significant improvement in heat transfer coefficient with trip height. In this figure the heat transfer coefficient was normalized to the air-water wetted area of the channels.

Results from Measurement #2

The results of Measurement #2 are listed in Table VII, showing that radiator #5 had an average overall heat transfer coefficient of 1478 W/(m^2 °C). Figure 19 shows that the overall heat transfer coefficient of radiator #5 varied little with water flow rate, suggesting that the rate of heat transfer under these conditions was largely air side limited. A linear fit to the data in figure 19 gives an average rate of change in the overall heat transfer coefficient as a function of water flow rate of 140 W/(m^2 °C)/(L/min) for water flow rates between 0.75 and 2.00 L/min. This is a variation of only 11% over the range of coolant flow rates planned for the Ion Tiger cooling system.

TABLE VII. Overall heat transfer coefficient for radiator #5 with a free stream air speed of 27 knots.

Coolant flowrate [L/min]	Coolant temperature change [°C]	Air inlet temperature [°C]	Average coolant temperature [°C]	U_{rad} [W/(m^2 °C)]
0.75 ± 0.06	3.3 ± 1.5	29 ± 1	62.3 ± 0.7	1384
1.00	2.7	29	64.7	1407
1.25	2.3	29	65.1	1481
1.50	2.0	29	65.6	1524
1.75	1.7	29	66.2	1487
2.00	1.6	29	66.8	1573
Average				***1478***

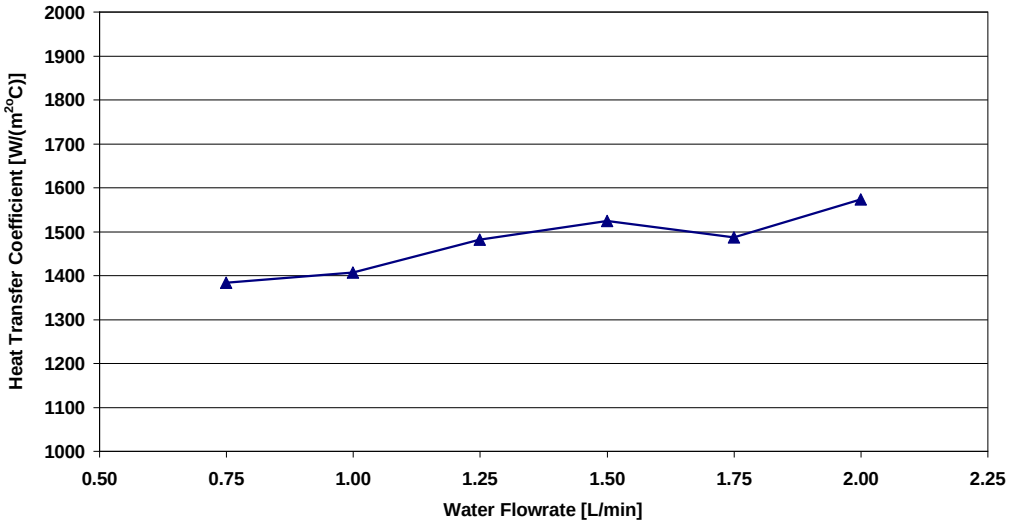

Figure 19. Variation in the overall heat transfer coefficient of radiator #5 with coolant flow rate.

Results from Measurement #3

The overall heat transfer coefficient of radiator #6 was measured at three water flow rates: 0.57, 0.75 and 0.90 L/min. The volumetric air flow rate through the radiator was 47 ft^3/min. The overall heat transfer coefficients based on the water and air side energy balances were 444 W/(m^2 °C) and 393 W/(m^2 °C) respectively. Since the average parameter r in equation 9 was 1.41, the heat transfer coefficients were computed using the arithmetic mean water and air temperatures instead of the LMTD. The average air side heat transfer coefficient agreed with the average water side to within 15%. The results are summarized in Table VIII. Referring to figure 13, the air side pressure drop across radiator #6 at this air flow rate was less than 0.18 in_{H2O}.

TABLE VIII. Overall heat transfer coefficients for radiator #6 at 47 ft^3/min air flow rate, using the arithmetic average temperatures.

Coolant flowrate [L/min]	Coolant temp change [°C]	Air temp change [°C]	Average coolant temp [°C]	Average air temp [°C]	U_{rad} water side [W/(m^2 °C)]	U_{rad} air side [W/(m^2 °C)]
0.57 ± 0.06	5.7 ± 1.5	6.1 ± 1.5	59.5 ± 0.7	28.3 ± 0.7	448	463
0.75	4.5	5.9	60.7	28.6	452	348
0.90	3.7	6.7	61.4	28.4	434	370
Averages					***444***	***393***

The overall heat transfer coefficients of radiator #7 measured at 29 ft^3/min and 34 ft^3/min air flow rates were 1534 W/(m^2 °C) and 1747 W/(m^2 °C) respectively. The LMTD was used to compute the heat transfer coefficients because $r > 5$. The average air and average water side measurements agreed to within 2% for the 34 ft^3/min air flow rate measurements and 1% for the 29 ft^3/min air flow rate. The full results are listed in Tables IX and X.

TABLE IX. Overall heat transfer coefficients for radiator #7 at 29 ft^3/min air flow rate, using the LMTD method.

Coolant flowrate [L/min]	Coolant temp change [°C]	Air temp change [°C]	Average coolant temp [°C]	Average air temp [°C]	U_{rad} water side [W/(m^2 °C)]	U_{rad} air side [W/(m^2 °C)]
1.00 ± 0.06	4.7 ± 1.5	35.0 ± 1.5	62.8 ± 0.7	35.0 ± 0.7	1513	1580
1.25	5.3	35.1	62.4	35.1	1562	1610
1.50	6.0	35.0	62.0	35.0	1578	1571
1.75	7.4	34.1	61.1	34.1	1496	1486
2.00	8.7	32.3	60.2	32.3	1478	1462
Averages					***1525***	***1542***

TABLE X. Overall heat transfer coefficients for radiator #7 at 34 ft^3/min air flow rate, using the LMTD method.

Coolant flowrate [L/min]	Coolant temp change [°C]	Air temp change [°C]	Average coolant temp [°C]	Average air temp [°C]	U_{rad} water side [W/(m^2 °C)]	U_{rad} air side [W/(m^2 °C)]
1.00 ± 0.06	4.7 ± 1.5	35.0 ± 1.5	62.8 ± 0.7	35.0 ± 0.7	1880	1844
1.25	5.3	35.1	62.4	35.1	1819	1864
1.50	6.0	35.0	62.0	35.0	1757	1710
1.75	7.4	34.1	61.1	34.1	1771	1688
2.00	8.7	32.3	60.2	32.3	1595	1543
Averages					***1764***	***1730***

The overall heat transfer coefficients for radiator #8 at 29, 31, 34 and 38 ft^3/min air flow rates are listed in Tables XI through XV. The LMTD was used again because $r > 4$ for all of the radiator # 8 measurements. It is not clear from the tables, but radiator #8 had a similar heat transfer coefficient to radiator #7. The values in Tables IX and XII and Tables X and XV differ despite having the same volumetric air flow rates because the air flows were distributed over different areas, leading to different air velocities. Plotting the overall heat transfer coefficients of each radiator as functions of the air velocity showed that they had similar heat transfer coefficients (see figure 20) because the data lie on the same line. This similarity was expected because both radiators had the same core geometry. The averages of the water and air side heat transfer coefficients agreed to within 15% for all air flow rates except for the 15 ft^3/min case were the discrepancy was 27%.

TABLE XI. Overall heat transfer coefficients for radiator #8 at 15 ft^3/min air flow rate, using the LMTD method.

Coolant flowrate [L/min]	Coolant temp change [°C]	Air temp change [°C]	Average coolant temp [°C]	Average air temp [°C]	U_{rad} water side [W/(m^2 °C)]	U_{rad} air side [W/(m^2 °C)]
1.00 ± 0.06	3.8 ± 1.5	29.6 ± 1.5	62.6 ± 0.7	36.4 ± 0.7	404	308
1.25	3.7	29.5	62.6	36.4	421	318
1.50	3.2	29.7	63.0	36.8	446	325
1.75	2.8	29.8	63.2	36.6	440	322
2.00	2.7	30.1	63.4	36.7	489	323
Averages					***440***	***319***

TABLE XII. Overall heat transfer coefficients for radiator #8 at 29 ft^3/min air flow rate, using the LMTD method.

Coolant flowrate [L/min]	Coolant temp change [°C]	Air temp change [°C]	Average coolant temp [°C]	Average air temp [°C]	U_{rad} water side [W/(m^2 °C)]	U_{rad} air side [W/(m^2 °C)]
1.00 ± 0.06	6.2 ± 1.5	28.6 ± 1.5	61.2 ± 0.7	35.9 ± 0.7	835	698
1.25	6.2	30.3	61.4	36.8	805	685
1.50	5.2	30.8	61.8	37.2	776	675
1.75	4.7	31.8	62.1	37.2	756	644
2.00	4.2	31.9	62.5	37.6	666	567
Averages					***767***	***654***

TABLE XIII. Overall heat transfer coefficients for radiator #8 at 31 ft^3/min air flow rate, using the LMTD method.

Coolant flowrate [L/min]	Coolant temp change [°C]	Air temp change [°C]	Average coolant temp [°C]	Average air temp [°C]	U_{rad} water side [W/(m^2 °C)]	U_{rad} air side [W/(m^2 °C)]
1.00 ± 0.06	7.9 ± 1.5	28.1 ± 1.5	61.6 ± 0.7	35.7 ± 0.7	642	597
1.25	6.0	28.6	61.4	35.0	612	614
1.50	5.4	30.0	64.4	36.6	666	651
1.75	4.3	30.0	62.7	36.3	678	712
2.00	4.2	32.4	65.7	36.8	697	727
Averages					***659***	***660***

TABLE XIV. Overall heat transfer coefficients for radiator #8 at 34 ft^3/min air flow rate, using the LMTD method.

Coolant flowrate [L/min]	Coolant temp change [°C]	Air temp change [°C]	Average coolant temp [°C]	Average air temp [°C]	U_{rad} water side [W/(m^2 °C)]	U_{rad} air side [W/(m^2 °C)]
1.00 ± 0.06	7.3 ± 1.5	30.1 ± 1.5	60.3 ± 0.7	36.2 ± 0.7	650	650
1.25	5.6	30.9	61.4	36.4	624	661
1.50	4.6	32.2	62.0	37.4	679	755
1.75	3.8	32.2	62.3	37.5	668	760
2.00	3.2	32.5	62.2	37.9	667	805
Averages					***658***	***726***

TABLE XV. Overall heat transfer coefficients for radiator #8 at 38 ft^3/min air flow rate, using the LMTD method.

Coolant flowrate [L/min]	Coolant temp change [°C]	Air temp change [°C]	Average coolant temp [°C]	Average air temp [°C]	U_{rad} water side [W/(m^2 °C)]	U_{rad} air side [W/(m^2 °C)]
1.00 ± 0.06	7.7 ± 1.5	31.1 ± 1.5	60.6 ± 0.7	36.8 ± 0.7	976	848
1.25	7.5	30.1	60.8	36.7	954	855
1.50	6.3	30.1	61.4	36.8	899	814
1.75	5.6	30.6	61.7	37.0	858	786
2.00	4.9	30.0	61.8	37.1	841	817
Averages					***905***	***824***

TABLE XVI. Summary of water-air average overall heat transfer coefficients for radiator #8 at several air flow rates.

Air flowrate [ft^3/min]	Calculated average air velocity through radiator [m/s]	U_{rad} water side [W/(m^2 °C)]	U_{rad} air side [W/(m^2 °C)]	U_{rad} water-air average [W/(m^2 °C)]
15 ± 1	0.24	440	319	380
29	0.44	767	654	710
31	0.47	659	660	660
34	0.52	658	726	707
38	0.58	905	824	864

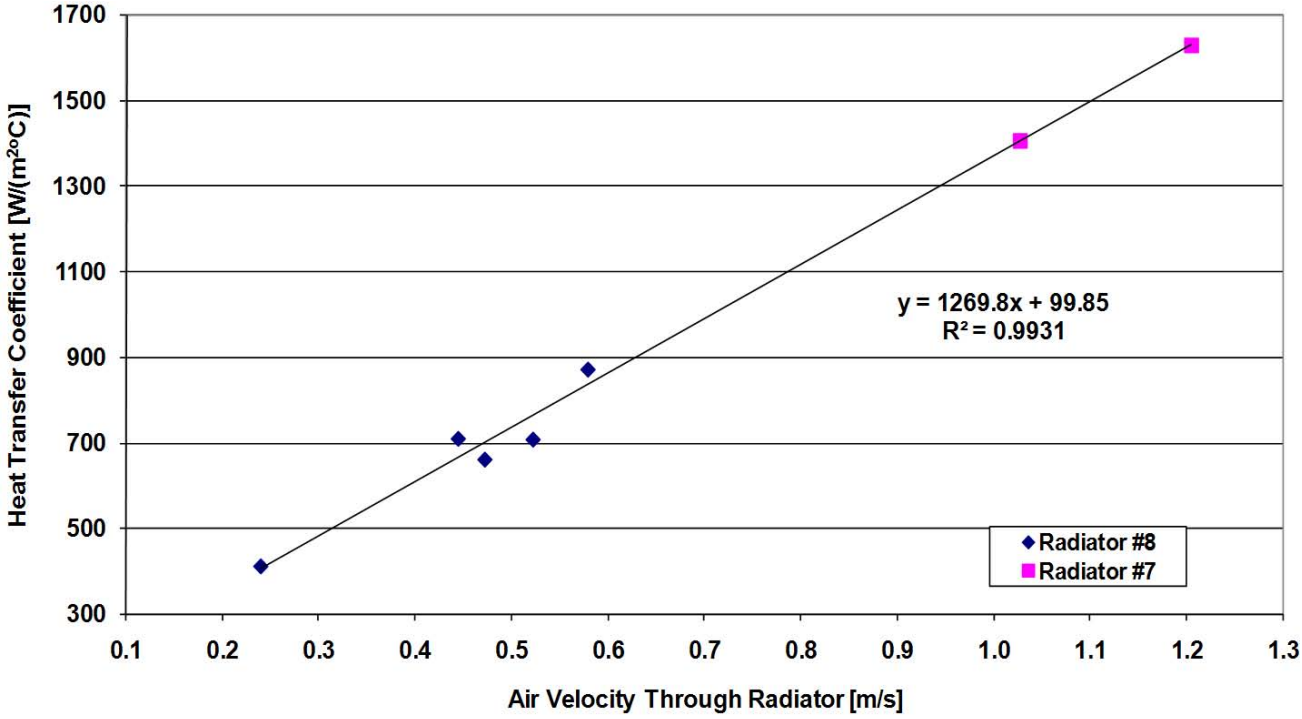

Figure 20. Radiator #7 and #8 overall heat transfer coefficients as functions of air velocity through the radiator. The line is a linear fit to the data.

Results from Measurement #4

The overall heat transfer coefficient for radiator #9 in the wind tunnel was 2142 W/(m^2 °C) with a free stream air speed of 27 knots. The heat transfer coefficient based on the water side energy balance in the bench top apparatus was 2302 W/(m^2 °C). The heat transfer coefficient based on the air side energy balance was 2458 W/(m^2 °C). The air and water side values agree to within 6%. The similarity of the wind tunnel and bench top values suggest that the pressure driving air flow through the radiator in each case was similar. Thus it was valid to compare the wind tunnel and bench top heat transfer results. See Tables XVII and XVIII for details.

TABLE XVII. Overall heat transfer coefficient for radiator #9, measured in the wind tunnel with a free stream air speed of 27 knots.

Coolant flowrate [L/min]	Coolant temp change [°C]	Air inlet temp [°C]	Average coolant temp [°C]	U_{rad} [W/(m^2 °C)]
1.00 ± 0.06	10.2 ± 1.5	29 ± 1	39.6 ± 0.7	1840
1.25	8.4	29	39.4	1931
1.50	7.2	30	39.5	2174
1.75	6.4	30	39.2	2328
2.00	5.8	30	39.1	2438
Average				***2142***

TABLE XVIII. Overall heat transfer coefficients for radiator #9, measured in the bench top apparatus at 59 ft^3/min air flow rate.

Coolant flowrate [L/min]	Coolant temp change [°C]	Air temp change [°C]	Average coolant temp [°C]	Average air temp [°C]	U_{rad} water side [W/(m^2 °C)]	U_{rad} air side [W/(m^2 °C)]
1.00 ± 0.06	15.6 ± 1.5	20.6 ± 1.5	52.2 ± 0.7	32.4 ± 0.7	2250	2510
1.25	13.5	22.2	55.0	33.6	2257	2478
1.50	11.9	23.4	56.4	34.0	2281	2445
1.75	10.5	24.3	57.4	34.5	2292	2428
2.00	9.7	24.5	57.7	34.9	2430	2430
Averages					***2302***	***2458***

One final note regarding Measurement #4: while heat transfer in the bench top test was clearly air limited, in the wind tunnel it was not (see figure 21). The most likely cause of this difference was the water temperature, which was much higher in the bench top testing.

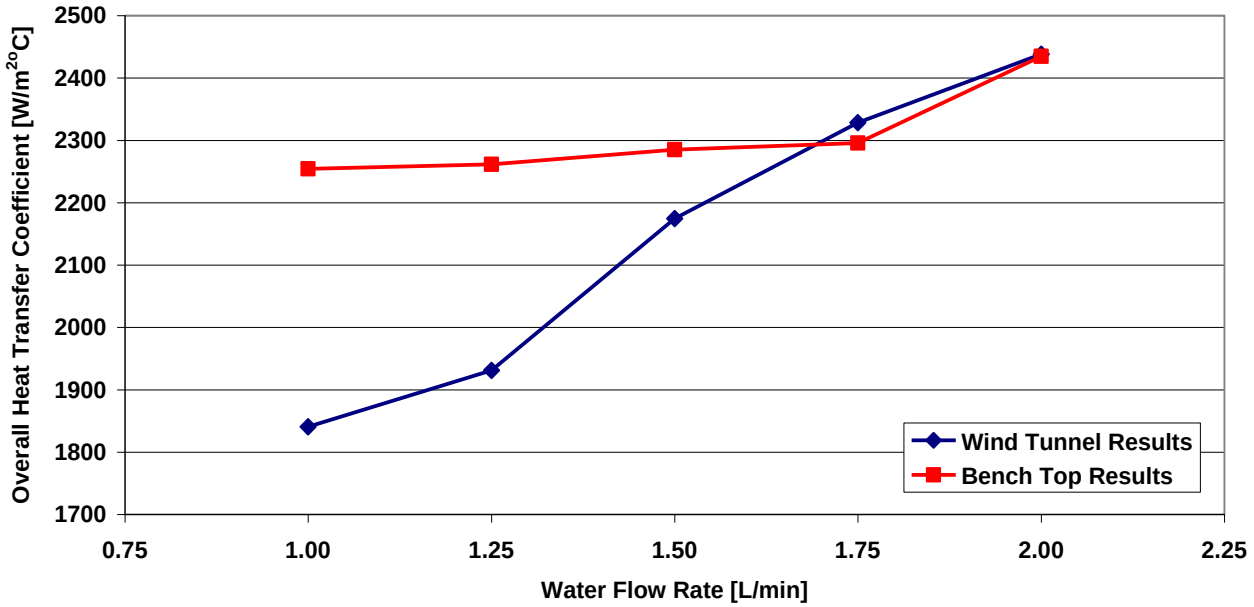

Figure 21. Radiator #9 overall heat transfer coefficient variation with coolant flow rate.

Results from Measurement #5

The highest pressure drops were in radiators #5 and #6 because they each had a single coolant flow channel. Radiators #7, #8 and #9 had many parallel channels and thus smaller coolant pressure drops. The water side pressure drops as functions of flow rate for radiators #5, #6, #7 and #9 are shown in figure 22. Radiators #7 and #8 both satisfied the required 1 lb/in^2 or less coolant pressure drop at 2.0 L/min flow rate.

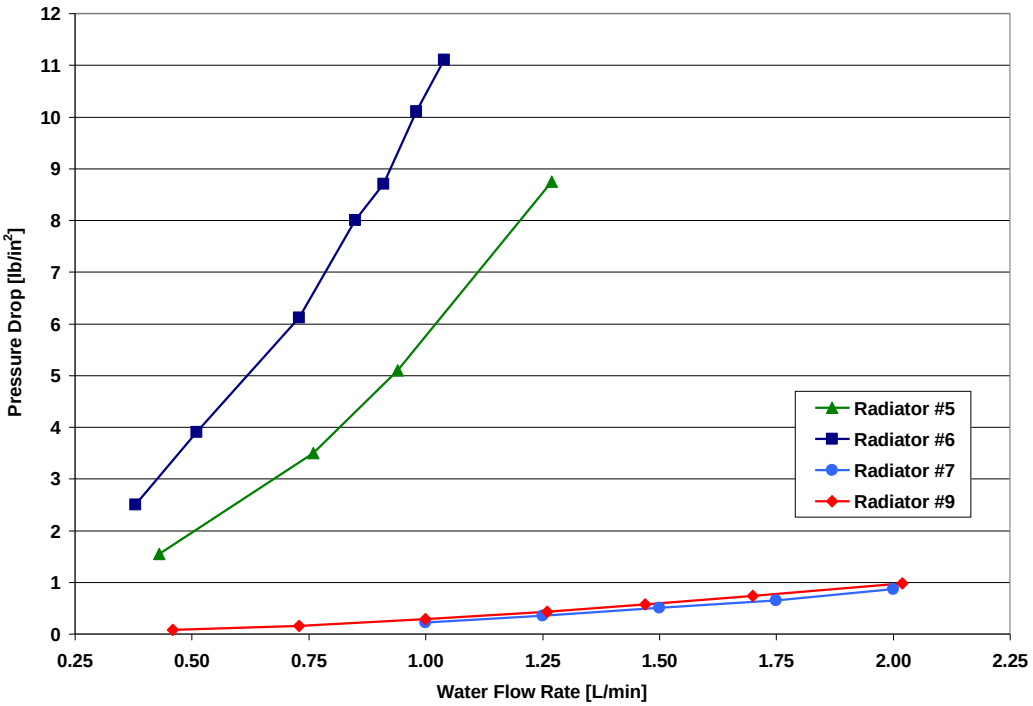

Figure 22. Water side pressure drop through radiators as a function of water flow rate. Uncertainty is ±0.03 lb/in^2.

Radiator and Fuel Cell Stack Models

Models were developed to choose a radiator design, size it to meet the Ion Tiger requirements and then predict its performance. A simple surface radiator model was created and validated by the results of Measurement #1. An empirical compact heat exchanger model was created based on the results of Measurement #3. An energy balance model of the fuel cell stack was created to predict the rate of heat rejection that would be required. The heat rejection rate was used with the two radiator models to predict the radiator mass of each that would be required to cool the Ion Tiger. Based on this calculation, a compact heat exchanger was chosen. The stack model was then coupled with the compact heat exchanger model to predict the performance of a radiator like #7 or #8 in the Ion Tiger.

Surface Radiator Model

The flat surface radiator model first discretizes the radiator in the direction of air and water flow, then computes the Reynolds number of the airflow at each cell based on distance x from the leading edge of the boundary layer plate. Equation 14 is then used to compute a local Nusselt number [1] for each cell, where ξ is the unheated starting length of the plate (see figures 23 and 24).

$$Nu_x = 0.0287\,\mathrm{Pr}^{0.6}\,\mathrm{Re}_x^{0.8}\left[1-\left(\frac{\xi}{x}\right)^{0.9}\right]^{-\frac{1}{9}} \qquad [14]$$

The local Nusselt number was used in equation 14 to compute the local heat transfer coefficient h_x at each point along the plate.

$$h_x = \frac{Nu_x k}{x} \qquad [15]$$

The local heat transfer coefficient was used to compute the local heat flux $\dot{q}_s''$ from each cell to the air in equation 15.

$$\dot{q}_s'' = h_x\left(T_s(x) - T_{air}\right) \qquad [16]$$

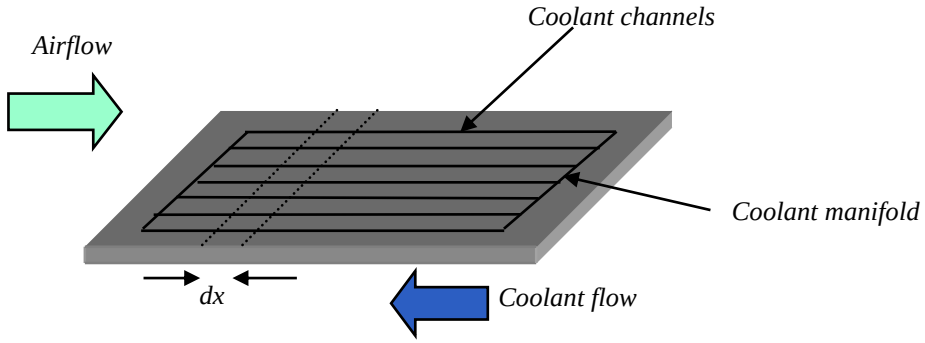

Figure 23. Discretization of the flat plate radiator in the direction of air and water flow.

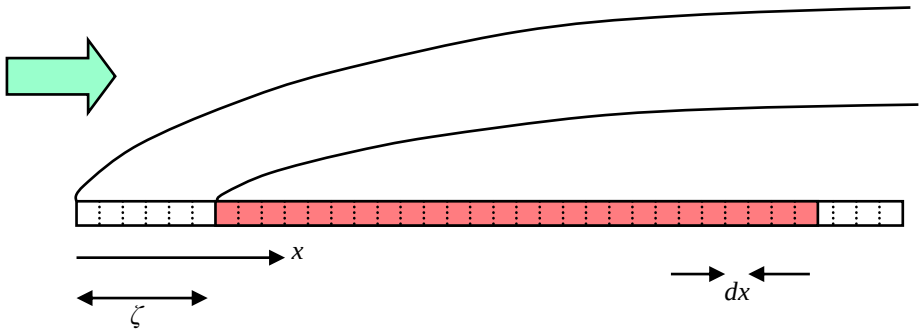

Figure 24. Schematic for calculating the local Nusselt number of each cell along the length of the radiator.

A similar process was used to compute the water side heat flux in each cell, although the water was laminar for all of the flow rates the Ion Tiger coolant pumps could generate, so a simpler local Nusselt number correlation was used. See figure 25 for the predicted plate heat flux as a function of distance from the leading edge of the plate.

The local heat fluxes were computed iteratively, adjusting the radiator surface temperature $T_s(x)$ until the heat flux from the water equaled the heat flux to the air over each cell. All of the local heat fluxes could then be summed to compute the total heat rejection in equation 17.

$$\dot{Q}_{rad} = \int_{\xi}^{L} h_x\left(T_s(x) - T_{air}\right)dx \qquad [17]$$

The heat transfer coefficient of each flat plate radiator could be predicted using equations 16 and 4, but it was not clear whether the entire cell area or only the air-aluminum-water area of the radiator surface should have been included. This decision hinged on the distance heat spread laterally from the channels into the aluminum sheet. Comparison to the experimental data showed that assuming the plate temperature was uniform laterally (the entire cell had the same temperature) produced a discrepancy of 5 – 20% between the model and experiments. Normalizing to the air-aluminum-water area produced much larger errors. This suggested that the consistent surface temperature assumption most closely represented the surface radiators in Measurement #1.

The 5 – 20% discrepancy was likely due to a combination of measurement error and deviations from the consistent temperature assumption. This matches intuition; for heat to flow into the aluminum there must have been a temperature gradient, thus some lateral variation in surface temperature must have been present.

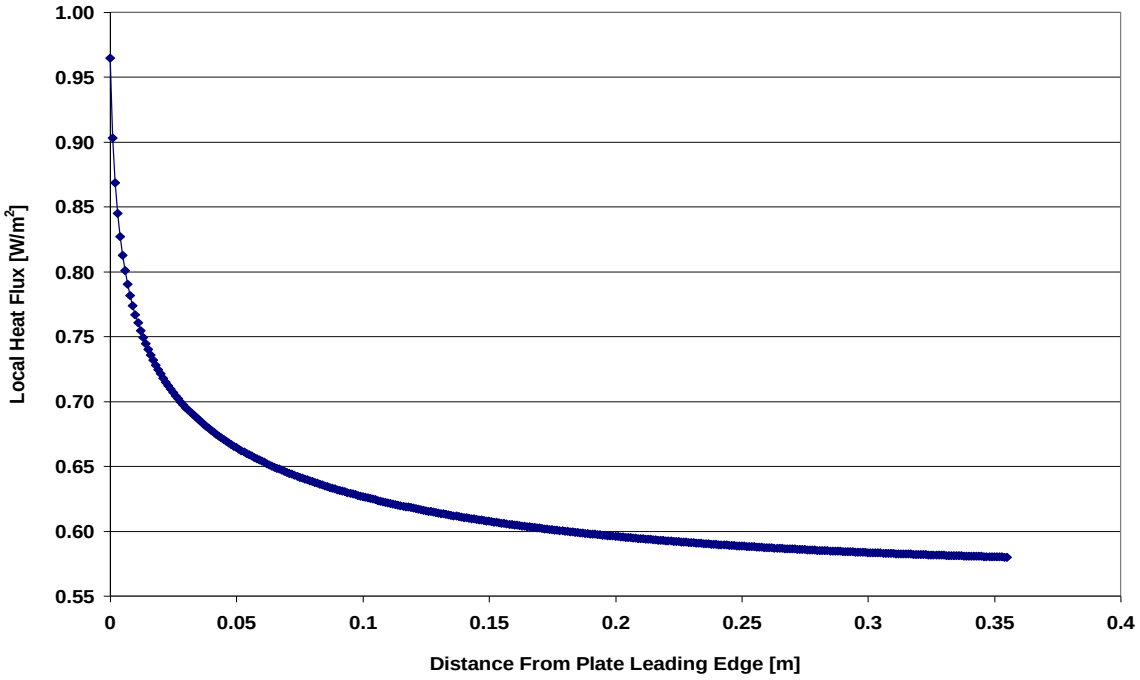

Figure 25. Calculated local heat flux along the length of the parallel channel flat plate radiator when $T_{coolant,in}$ = 71.6 °C, $T_{coolant,out}$ = 64.0 °C, and T_{air} = 20.7 °C.

Compact Heat Exchanger Model

The curve in figure 20 was used to create a simple empirical LMTD model of radiators #7 and #8. Equations 18 and 19 describe the overall heat transfer coefficient in terms of air velocity through the radiator (equation 17) or in terms of the air volumetric flow rate and radiator area (equation 19). Equations 18 and 19 are only valid for values near those that were measured; i.e. water flow rates between 1.0 and 2.0 L/min and air flow velocities between 0.2 and 1.2 m/s. At some point beyond these ranges the curve becomes non-linear and the model is no longer accurate.

$$U_{rad}(v_{air}) = 1269\left[\frac{\mathrm{W\,s}}{\mathrm{m^3\,^\circ C}}\right] v_{air}\left[\frac{\mathrm{m}}{\mathrm{s}}\right] + 99.9\left[\frac{\mathrm{W}}{\mathrm{m^2\,^\circ C}}\right] \quad [18]$$

$$U_{rad}(\dot{V}, A_{rad}) = \frac{\dot{V}\left[\frac{\mathrm{ft^3}}{\mathrm{min}}\right]}{1.670\left[\frac{\mathrm{ft^3\,^\circ C}}{\mathrm{W\,min}}\right] A_{rad}\left[\mathrm{m^2}\right]} + 99.9\left[\frac{\mathrm{W}}{\mathrm{m^2\,^\circ C}}\right] \quad [19]$$

Fuel Cell Energy Balance Model

The thermal load must be known in order to select a radiator design and size it properly. For the Ion Tiger, the thermal load was defined as the rate at which heat must be rejected for the fuel cell system to operate indefinitely at full power in 38 °C ambient conditions. Waste heat is generated by several inefficiencies inherent to PEMFC operation and by water vapor condensing in the stack. The coolant, the cathode exhaust and the hydrogen purge all remove heat from the stack (convection and radiation to the environment are insignificant). There are two steps in determining the radiator thermal load; predicting the total rate of heat waste heat production by the fuel cell and determining the portion removed by the coolant.

Fuel Cell Energy Balance Model Background

Determining the rate of waste heat production begins with the overall reaction taking place in the fuel cell (equation 20):

$$2H_2 + O_2 \rightarrow 2H_2O \qquad [20]$$

Equation 20 is the sum of equations 21 and 22, which take place on the anode and cathode sides of the membrane:

$$\text{Anode:} \quad H_2 \rightarrow 2H^+ + 2e^- \qquad \text{Cathode:} \quad O_2 + 4H^+ + 4e^- \rightarrow 2H_2O \qquad [21, 22]$$

Protons liberated on the anode by H_2 dissociation diffuse through the membrane to the cathode side due to the proton (or H_3O^+) concentration gradient. Electrons cannot diffuse though the membrane, so they flow through the external circuit in response to the difference in potential across the membrane. The potential across the membrane is the voltage V_{cell} of the fuel cell, and the flow of electrons through the external circuit I_{cell} is the current. The relationship between current and voltage in a PEMFC is often described by plotting V_{cell} vs. I_{cell}. This plot is called a polarization curve and has a distinctive shape governed by the loss mechanisms in a PEMFC. The polarization curve of the Ion Tiger fuel cell is given in figure 26.

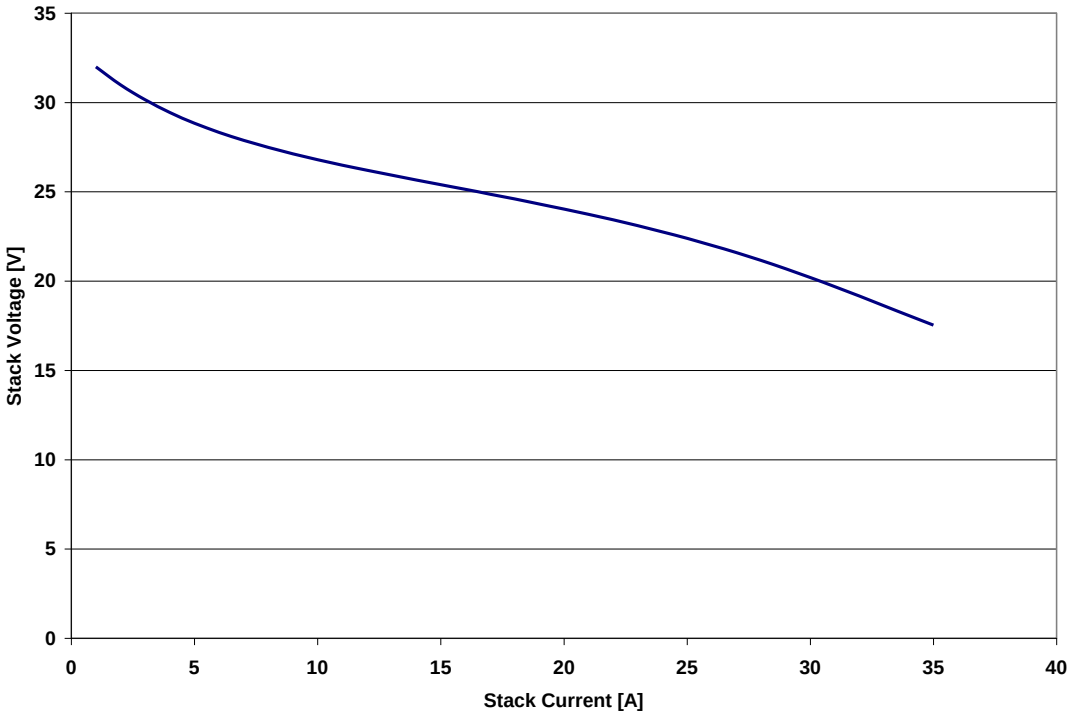

Figure 26. Ion Tiger fuel cell stack polarization curve.

The power output of the fuel cell is the product of current and voltage, so the polarization curve can be used to plot power output as a function of current output. Figure 27 shows is the Ion Tiger fuel cell power curve.

$$P_{cell} = I_{cell} V_{cell} \qquad [23]$$

The fuel cell current can be written in terms of the molar flowrate of electrons $\dot{n}_{elec}$ if the charge carried by each mole of electrons is accounted for. Multiplying by Faraday's constant (F = 96485 C/mol electrons) gives:

$$I_{cell} = \dot{n}_{elec} F \qquad [24]$$

The rate of waste heat production by a PEMFC depends both on the current (which describes the rate of reaction) and the voltage (which describes the level of inefficiency). Since the current and voltage are related by the polarization curve, the

rate of waste heat generation could be derived in terms of either parameter. Since aeronautical engineers are most interested in power, here the rate of waste heat production is derived in terms of fuel cell power output.

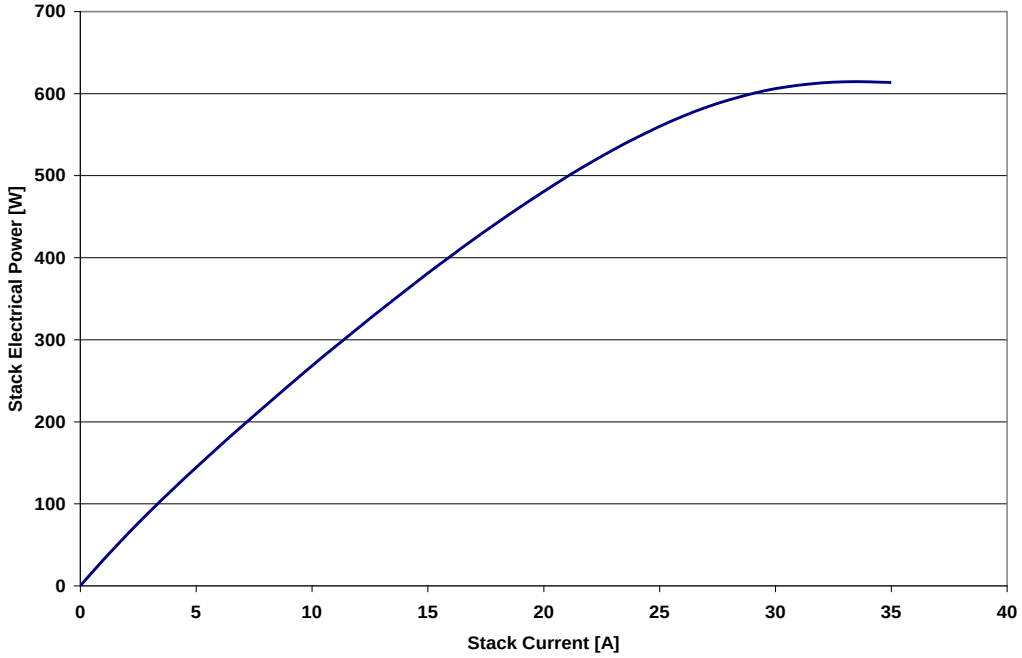

Figure 27. Ion Tiger fuel cell stack power curve.

Substituting equation 24 into equation 23 yields the power output of a single fuel cell in terms of electron flowrate and voltage across the cell:

$$P_{cell} = \dot{n}_{elec} F V_{cell} \qquad [25]$$

The reaction stoichiometry indicates that two hydrogen molecules and one oxygen molecule are consumed for every four electrons flowing through the external circuit. Combining this fact with equation 25, the reaction rates can be related to the electrical power output and cell voltage. The results are equations 26, 27 and 28.

$$\dot{n}_{H_2,cell} = \frac{P_{cell}}{2V_{cell}F} \quad , \quad \dot{n}_{O_2,cell} = \frac{P_{cell}}{4V_{cell}F} \quad , \quad \dot{n}_{H_2O,cell} = \frac{P_{cell}}{2V_{cell}F} \qquad [26, 27, 28]$$

To produce sufficient power, cells are normally combined to form a stack in which the cells are in series electrically and in parallel with respect to mass flows (reactants, products and coolant). For a stack of N cells the reaction rate is roughly the same in each cell, so the total molar flow rate for the stack will be a factor of N larger than that of a single cell. The total power output of the stack is the sum of the power produced by each cell, or $NP_{cell} = P_{stack}$. The stack molar flow rates are then given by equations 29, 30 and 31.

$$\dot{n}_{H_2} = \frac{P_{stack}}{2V_{cell}F} \quad , \quad \dot{n}_{O_2} = \frac{P_{stack}}{4V_{cell}F} \quad , \quad \dot{n}_{H_2O} = \frac{P_{stack}}{2V_{cell}F} \qquad [29, 30, 31]$$

The full power flow rates are a good point of reference. The designed electrical full power gross output of the Ion Tiger stack is P_{elec} = 600 W, at which point the voltage has been drawn down to approximately V_{stack} = 21 V (see figures 26 and 27). There are 36 cells in the stack, so the average voltage per cell at full power is V_{cell} = 21 V/36 cells = 0.58 V/cell. The maximum reaction rates computed by using these values in equations 29, 30 and 31 are listed in Table XIX.

TABLE XIX. Ion Tiger reactant consumption and product formation rates at full power (600 W stack gross output).

Reactant/Product	Full Power Rate [mol/hr]	Full Power Rate [g/hr]
Hydrogen	19.3	38.6
Oxygen	9.7	310.4
Water	19.3	347.4

An energy balance on the fuel cell stack can be used to determine the rate of heat rejection to the coolant if it is the only unknown term. With the reaction rates from equations 29, 30 and 31 and some educated assumptions regarding the states of the fuel cell and inlet and outlet streams, the coolant enthalpy is the only unknown term.

Engineering Equation Solver (EES) was used to solve the stack energy balance for the rate of heat rejection. EES was chosen because its built-in JANNAF tables simplified the evaluation of fluid thermodynamic properties. Seven energy flows into and out of the stack were included: the enthalpies of the H_2 inlet, H_2 purge, cathode inlet, cathode exhaust vapor, cathode exhaust liquid, coolant inlet, coolant outlet, and the electrical power out (see figure 28). The stack was assumed to be adiabatic aside from the seven aforementioned flows and the system was assumed to be at steady state. The complete energy balance is given in equation 32.

$$0 = \left(P_{elec} + h_{H_2,out}\dot{n}_{H_2,out} + h_{cathodegas,out}\dot{n}_{cathodegas,out} + h_{cathodeliq,out}\dot{n}_{cathodeliq,out} + \dot{Q}_{rad}\right) - \left(h_{cathodein}\dot{n}_{cathodein} + h_{H_2,in}\dot{n}_{H_2,in} + h_{reaction}\dot{n}_{H_2O}\right) \quad [32]$$

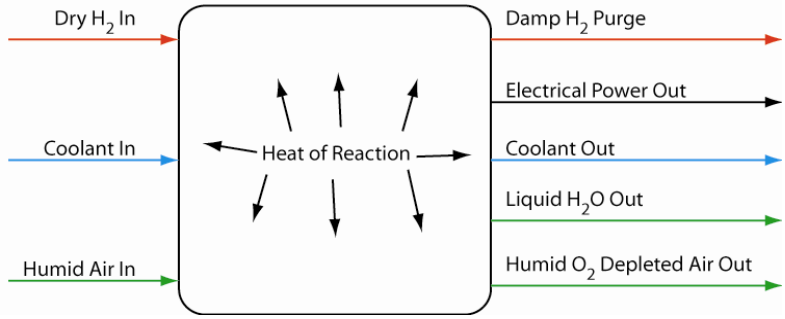

Figure 28. Complete fuel cell stack energy balance, in which each mass flow has an enthalpy and flow rate.

The following list explains each term in equation 32, in order from left to right. Each term had units of power [W]. The "stack temperature" was always taken to be the coolant temperature as it entered the stack.

- P_{elec} : The rate of electrical energy production. The stack voltage at a given power output was estimated by polynomial fits to the power and polarization curves in figures 26 and 27.
- $h_{reaction}\dot{n}_{H_2O}$: The rate at which chemical energy in the reactants was converted into electricity and heat. The molar specific chemical energy made available by the reaction ($h_{reaction}$) was the enthalpy of formation for water. The value of $h_{reaction}$ for gas phase reactants and products (241,800 J/mol) was used because condensation was accounted for in the cathode outlet enthalpy calculation. Equation 31was used to compute the rate of water production ($\dot{n}_{H_2O}$).
- $h_{H_2,out}\dot{n}_{H_2,out}$: The rate at which enthalpy was carried out of the stack by purged hydrogen. The molar specific enthalpy ($h_{H_2,out}$) was computed at the stack temperature and anode pressure. The molar flow rate of H_2 out of the stack ($\dot{n}_{H_2,out}$) was the product of the fuel utilization (η_{fuel}) and the molar flow rate of fuel entering the stack (see equation 33). H_2 at the anode outlet was assumed to be dry, although in a real system some fraction of the product water would be expected to emerge from the anode due to back diffusion through the membranes.

$$\dot{n}_{H_2,out} = \dot{n}_{H_2,in}\left(1 - \eta_{fuel}\right) \quad [33]$$

- $h_{cathodegas,out}\dot{n}_{cathodegas,out}$ and $h_{cathodeliq,out}\dot{n}_{cathodeliq,out}$: The rates at which enthalpy was carried out of the stack by the gaseous and liquid components of the cathode flow. The molar specific enthalpies ($h_{cathodegas,out}$ and $h_{cathodeliq,out}$) were those for saturated air and liquid water, respectively. The enthalpies were computed at the stack coolant outlet temperature and ambient pressure. The cathode exhaust gas was assumed to have the same

thermodynamic properties as humid air (density, specific heat, etc.) despite the reduced O_2 concentration. The cathode exhaust gas and liquid flow rates were computed by comparing the actual water mass fraction to the possible saturated water mass fraction; any water beyond the saturated water mass fraction was assumed to be liquid. The cathode outlet gas flow rate ($\dot{n}_{cathode,gas,out}$) was the inlet air flow rate minus the inlet water vapor flow rate, minus the rate of O_2 consumption, plus the water vapor to saturate the flow (see equation 34).

$$\dot{n}_{cathode,gas,out} = \dot{n}_{cathode,in} - \dot{n}_{H_2O,vap,in} - \dot{n}_{O_2} + \dot{n}_{H_2O,vap,out} \quad [34]$$

The cathode outlet liquid flow rate ($\dot{n}_{cathode,liq,out}$) was the water production rate plus the rate of water vapor entering the stack, minus the rate at which the cathode outlet gas flow could carry water vapor (see equation 35).

$$\dot{n}_{cathode,liq,out} = \dot{n}_{H_2O} + \dot{n}_{H_2O,vap,in} - \dot{n}_{H_2O,vap,out} \quad [35]$$

- $\dot{Q}_{rad}$: The rate of heat rejection to the radiator. It was the difference in the rates at which coolant carries enthalpy into and out of the stack, which were computed using equation 4.
- $h_{cathode,in}\dot{n}_{cathode,in}$: The rate at which enthalpy was carried into the stack by the cathode inlet flow. The molar enthalpy of the flow ($h_{cathode,in}$) was determined at the cathode inlet temperature, cathode inlet pressure, and the cathode inlet relative humidity $RH_{cathode,in}$. The inlet cathode air passes through a counter flow membrane exchanger where it absorbs heat and moisture from the cathode outlet flow (see figure 29). The cathode inlet temperature was computed as the average of the ambient air and the cathode outlet temperatures (see equation 36). The fuel cell vendor, Protonex, indicated that the air relative humidity is typically 0.50 – 0.75 when it leaves the humidifier and enters the stack. For worst-case calculations the cathode inlet relative humidity was set to 1.0, otherwise it was assumed to be 0.75.

$$T_{cathode,in} = \tfrac{1}{2}\left(T_{cathode,out} + T_{ambient}\right) \quad [36]$$

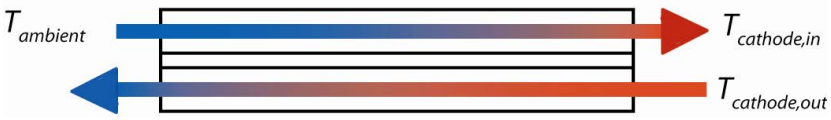

Figure 29. Fuel cell humidifier schematic.

The molar flow rate of air at the inlet ($\dot{n}_{cathode,in}$) was set to 30 SL/min (the maximum value) for worst case calculations and a value between 0 – 30 SL/min for other simulations, with a stoichiometry of roughly 2.

- $h_{H_2,in}\dot{n}_{H_2,in}$: The rate at which enthalpy was carried into the stack by the hydrogen flow. The H_2 was assumed to enter the stack dry, so the molar enthalpy ($h_{H_2,in}$) was simply evaluated at ambient temperature and the anode pressure. The molar flow rate of H_2 was the sum of the rates of consumption and purging (see equation 37). The consumption rate was computed by equation 29.

$$\dot{n}_{H_2,in} = \dot{n}_{H_2,consumed} + \dot{n}_{H_2,out} \quad [37]$$

Two ancillary parameters were provided by the model in addition to the radiator heat rejection rate. The first was the thermal efficiency of the fuel cell. The thermal efficiency was defined as the useful electrical output compared to the total chemical energy liberated from the reactants. This provided a measure of how efficiently the fuel cell was converting fuel to electricity. Equation 38 defined stack thermal efficiency in this study.

$$\eta_{th} = \frac{P_{elec}}{P_{total}} = \frac{P_{elec}}{h_{reaction}\dot{n}_{H_2O}} \quad [38]$$

The second ancillary parameter was the rate of liquid water flowing out of the humidifier outlet ($\dot{n}_{H2O,humid,liq,out}$). Since liquid water rests on the membrane surface and water vapor may simply flow out of the humidifier, the water for humidifying the cathode inlet stream was assumed to come from the liquid fraction of the cathode outlet stream. The process in a real humidifier is more complex, but this assumption was expected to be reasonable. The rate of water consumption by the humidifier ($\dot{n}_{H2O,humid,consump}$) was computed using equation 39, where $\varphi_{cathode,in}$ was the humidity fraction of the cathode inlet flow and $\varphi_{ambient}$ was the humidity fraction of the ambient air. Humidity fractions were computed by EES based on the relative humidity, temperature and pressure of each flow. The rate at which liquid water flowed out of the humidifier was computed using equation 40.

$$\dot{n}_{H2O,humid,consump} = \phi_{cathode,in}\dot{n}_{cathode,in} - \phi_{ambient}\dot{n}_{humid,in} \quad [39]$$

$$\dot{n}_{H2O,humid,liq,out} = \dot{n}_{cathode,liq,out} - \dot{n}_{H2O,humid,consump} \quad [40]$$

The fuel cell system had a valve which allowed the control electronics to shunt some coolant from the stack outlet directly back to the inlet bypassing the radiator; this way the controls could maintain a minimum fuel cell stack temperature. The bypass valve servo received a signal from the control electronics telling it which position to take as a fraction of the maximum possible angular travel. The fraction of full bypass valve servo travel was included in the model as a parameter dictating the fraction of coolant which bypassed the radiator.

The fuel cell energy balance model consisted of 45 equations and 65 parameters, any of which could be specified or solved for, so long as 20 parameters were specified and 45 were unspecified. Specified parameters in this study included:

- The stack gross electrical power output
- The humidifier inlet (intake point for ambient air) volumetric flow rate, temperature, pressure and relative humidity
- The hydrogen inlet temperature and pressure
- The fuel utilization (fraction of fuel flow consumed by the reaction)
- The coolant inlet temperature, pressure and flowrate

Typical model outputs (parameters not specified by the user) were:

- The flow rates, states (temperature, pressure, quality) and energy carried by each of the outlet streams
- The rate of fuel consumption
- Stack thermal efficiency (defined below)

Radiator Heat Rejection Rate Predicted by the Fuel Cell Energy Balance Model

The fuel cell energy balance model was used to calculate the rate of heat rejection required of the radiator for many values of the fuel cell stack coolant inlet temperature. For each model calculation the radiator worst-case parameters in Table XX were used. The results in figure 30 show that as the stack is operated at higher temperatures, the heat the radiator must reject tends to decrease. This trend is attributable to the change in enthalpy of the cathode stream as it flows through the stack. At stack temperatures below ~60 °C, product water from the reaction is condensing as it is added to the cathode stream by the chemical reaction, which increases the radiator heat load. At ~60 °C water is evaporating at the same rate it is added; above ~60 °C the evaporating water carries away some of the heat load. Above ~70 °C all of the water added to the stack by the humidifier and chemical reaction leaves as vapor, so further increases in stack temperature provide little benefit by way of reducing the radiator heat load. The cathode inlet relative humidity was set to 1.0 in the worst case scenario because it created the greatest possible latent heat load on the radiator at all stack temperatures.

The slight rise in net heat rejection in figure 30 is due to the model assumption that the maximum cathode volumetric flowrate is fixed; this means that the mass flow rate falls as the stack temperature increases and the cathode stream capacity to reject heat decreases slightly. The rate of heat rejection by the anode was not included in figure 30 because it consistently removes only ~2 W.

The maximum stack operating temperature was set by the manufacturer at 70 °C because the membranes tend to dry out at higher temperatures. This makes sense in the context of figure 30; beyond ~70 °C the cathode stream relative humidity at the outlet falls below 1.0 and can remove water from the stack faster than it is flowing in and being generated. When the stack coolant inlet temperature is ~70 °C, the predicted radiator heat load is 466 W.

TABLE XX. Ion Tiger worst-case parameters used in the stack thermal model to predict the heat rejection rates in figure 30.

Parameter	Value
Fuel cell stack gross electrical power output	600 W
Ambient temperature	38 °C
Ambient pressure	101 kPa
Ambient relative humidity	0.40
Cathode inlet relative humidity	1.0
Cathode volumetric flow rate	30 L/min
Coolant flow rate	2.0 L/min
Fuel utilization	0.99

The fuel cell can operate at room temperature; however the peak power output is higher when the stack temperature is closer to ~55 °C. The minimum stack operating temperature (i.e. the minimum target temperature of the control electronics) was set at 54 °C. At this temperature the predicted radiator heat load was greatest (~800 W) given the normal fuel cell operating temperature range. Being the worst-case prediction, this heat load was used for the subsequent radiator sizing.

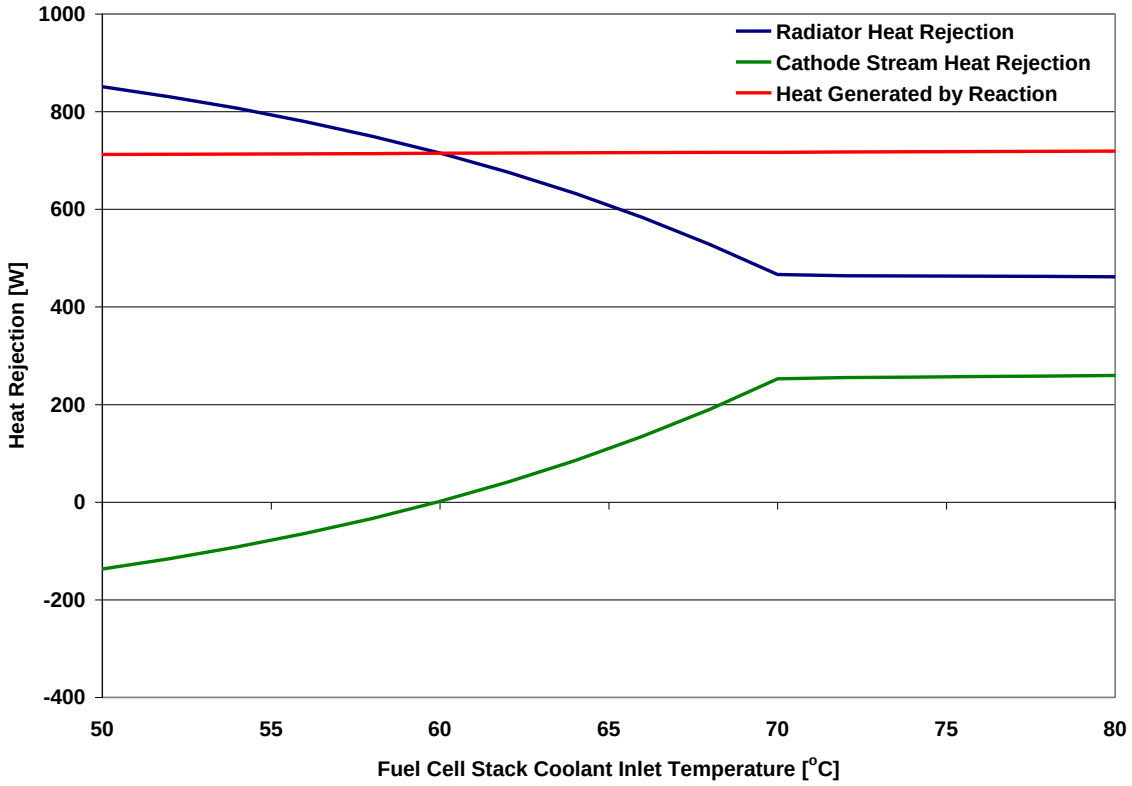

Figure 30. Rates of heat rejection by the cathode stream and radiator and the rate of heat production by the fuel cell at different stack coolant inlet temperatures, assuming full power operation. For rest of the parameters of this simulation, see Table XX.

Cooling System Design

The cooling system consisted of four main components: the radiator, fans, coolant pump and bypass valve. Protonex chose the cooling pump and designed the bypass valve; for the purposes of this study that portion of the cooling system was fixed. The radiator type with the highest heat transfer per unit weight was chosen by NRL, then sized to the predicted heat load. The fans and duct were designed once the radiator was sized. The complete system was later evaluated in a wind tunnel to verify the predicted performance.

A pump maintains coolant flow through the fuel cell at all times to minimize temperature gradients in the stack. The coolant flowrate is increased from a minimum value in proportion to the current output of the stack, assuming a linear relationship between current and the rate of waste heat production. While the coolant temperature at the fuel cell stack inlet is below a temperature set point, all of the coolant is recirculated from the outlet directly to the inlet without passing through the radiator. When the stack coolant inlet temperature exceeds the set point, the bypass valve directs a portion of the coolant flow through the radiator. If the stack temperature continues to rise, more coolant is directed through the radiator until the bypass valve reaches the fully open state. The cooling fans are turned on when the coolant temperature rises beyond a second, higher set point. Between the first and second temperature set points the bypass valve servo position is linearly related to coolant temperature: fully closed at the first set point and fully open at the second set point.

Selecting and Sizing a Radiator for the Ion Tiger

The measured characteristics of each radiator type were used to determine how much area (and weight) would be needed in order to cool the Ion Tiger. Equation 5 and the following parameters were used in these calculations:

- Overall heat transfer coefficient, U_{rad}, which was measured for each radiator (see Tables V to XVIII).
- Likely worst-case thermal load, Q_{rad}, which the stack thermal model predicted to be 800 W.
- Maximum coolant flow rate of 2 L/min. (see Table I).
- The worst-case inlet air temperature, $T_{air,in}$ = 38 °C (see Table I).
- Coolant inlet temperature, $T_{coolant,in}$ = 55.0 °C
- Coolant outlet temperature, $T_{coolant,out}$ = 60.8 °C, computed using equation 4.
- Radiator area density, ρ_{area}, which was measured for each radiator (see Tables II and III).
- Air speed over or through the radiator. For the surface radiators this was the Ion Tiger cruise speed of 27 knots (13.9 m/s) and for the CHEs this was 2.0 m/s.

Radiators #1 - #5

The required areas and masses of the radiators designed for the aircraft fuselage exterior are listed in Table XXI. The only surface radiator included in Table XXI was radiator #3, because it had the largest overall heat transfer coefficient based on the entire aluminum surface area. The smaller overall heat transfer coefficients of the other surface radiators would have made them larger and heavier than radiator #3. For the details see Appendix II, calculation #1.

TABLE XXI. Area and mass of the most effective surface radiator (radiator #3) and the one CHE designed for the outside of the aircraft fuselage (radiator #5), scaled to an 800 W cooling load for a fuel cell at 55 °C in 38 °C ambient air flowing at 27 knots. Masses do not include plumbing.

Radiator	Min Area [cm^2]	Minimum Area/Area of Measured Radiator	Wet Mass [g]
Radiator #3	3859	5.8	1019
Radiator #5	131	7.4	566

Almost six of radiator #3 and more than seven of radiator #5 would be required to cool the Ion Tiger. Since the overall heat transfer coefficients of these radiators changed little with coolant flow rate, this analysis would be accurate whether the hypothetical Ion Tiger versions of radiator #3 and #5 were plumbed in series or parallel on the coolant side. All of the surface radiators (#1 – #4) were eliminated from consideration because they exceeded the radiator weight limit (680 g, see Table I) and the Ion Tiger fuselage could not accommodate the required area. Radiator #5 was eliminated because it would have produced too much aerodynamic drag.

Radiator #6

The overall heat transfer coefficient of radiator #6 was lower than that of radiator #7, and the area density of radiator #6 was larger than that of radiator #7. These two comparisons ensure that to reject the same amount of heat under the same conditions, radiator #6 will always be larger and heavier than radiator #7, so radiator #6 was eliminated from consideration.

Radiators #7 and #8

The aircraft designers believed they could reasonably produce a fan assisted air velocity through an internal CHE of ~ 2 m/s. Using the empirical correlation for radiators #7 and #8 in equation 18, the result is a radiator which would have an area of 246 cm^2 and mass of 441 g. See Appendix II, calculation #3 for the process used to calculate these values.

The heat transfer characteristics/weight and /area of radiators #7 and #8 were superior to the other designs considered in this study. Radiator #8 as tested was estimated to provide a safety factor of ~1.25 for the expected worst case operating conditions of the Ion Tiger, so it was chosen for use in the airplane without modification.

Radiator #9

The relatively inefficient tanks on radiator #9 and made it heavier than radiators #7 and #8 for the same rate of heat transfer, so it was not considered for use in the Ion Tiger.

Cooling System Design Sensitivity Analysis

An overall cooling system model was created with the fuel cell stack energy balance model and the LMTD model of the Ion Tiger radiator as submodels. The two submodels were coupled by linking the coolant flow rates and temperatures; this way the radiator must reject heat to the air at the same rate the fuel cell rejects heat to the radiator.

Exploring the sensitivity of the final design to perturbations in the design variables is important because designs which depend heavily on one variable are prone to failure by design error. The combined fuel cell stack/radiator model was used to estimate the change in maximum ambient operating temperature for the Ion Tiger with changes in stack temperature, cathode inlet relative humidity (humidifier effectiveness) and radiator air speed. These variables were included in the sensitivity analysis because they played critical roles in the radiator sizing. The sensitivity to radiator area was also evaluated because it is the final "output variable" of the entire design process. Table XXII lists the model parameters used in the sensitivity simulations.

TABLE XXII. Parameters for the sensitivity analysis simulations. For each simulation, refer to the dependent variable in the simulation rather than the one in this table.

Parameter	Value
Fuel cell stack gross electrical power output	600 W
Fuel cell stack temperature at coolant inlet	65 °C
Ambient pressure	101 kPa
Ambient relative humidity	0.40
Cathode inlet relative humidity	1.0
Cathode volumetric flow rate	30 L/min
Coolant flow rate	2.0 L/min
Fuel utilization	0.99
Bypass fraction	0.00
Radiator air speed	5.35 m/s
Radiator area	304 cm^2
Radiator overall heat transfer coefficient	6888 W/(m^2 °C)

Figure 31 shows that raising the fuel cell coolant inlet temperature will raise the maximum ambient operating temperature for the Ion Tiger. This was the result of two phenomena at higher stack temperatures (1) the cathode removes more waste heat due to the greater rate of water evaporation in the stack and (2) the higher radiator temperature allows operation in warmer air with the same radiator-air temperature difference. The changing cathode inlet relative humidity in figure 32 was predicted to have little effect on the maximum ambient operating temperature because the coolant temperature at the fuel cell outlet rises to accommodate the latent heat load of additional condensation in the stack. Figures 33 and 34 show the same trends:

increasing the radiator heat transfer area and increasing the radiator air speed both increase the maximum ambient operating temperature, but with diminishing returns. The radiator area and the radiator air speed are inversely related to the ambient air temperature through equations 5 and 8, so increasing them causes the maximum ambient operating temperature to asymptotically approach a maximum value. Over the range of variation expected in these four variables, the Ion Tiger cooling system should satisfy the 38 °C minimum ambient temperature specification, and in most cases will far exceed it.

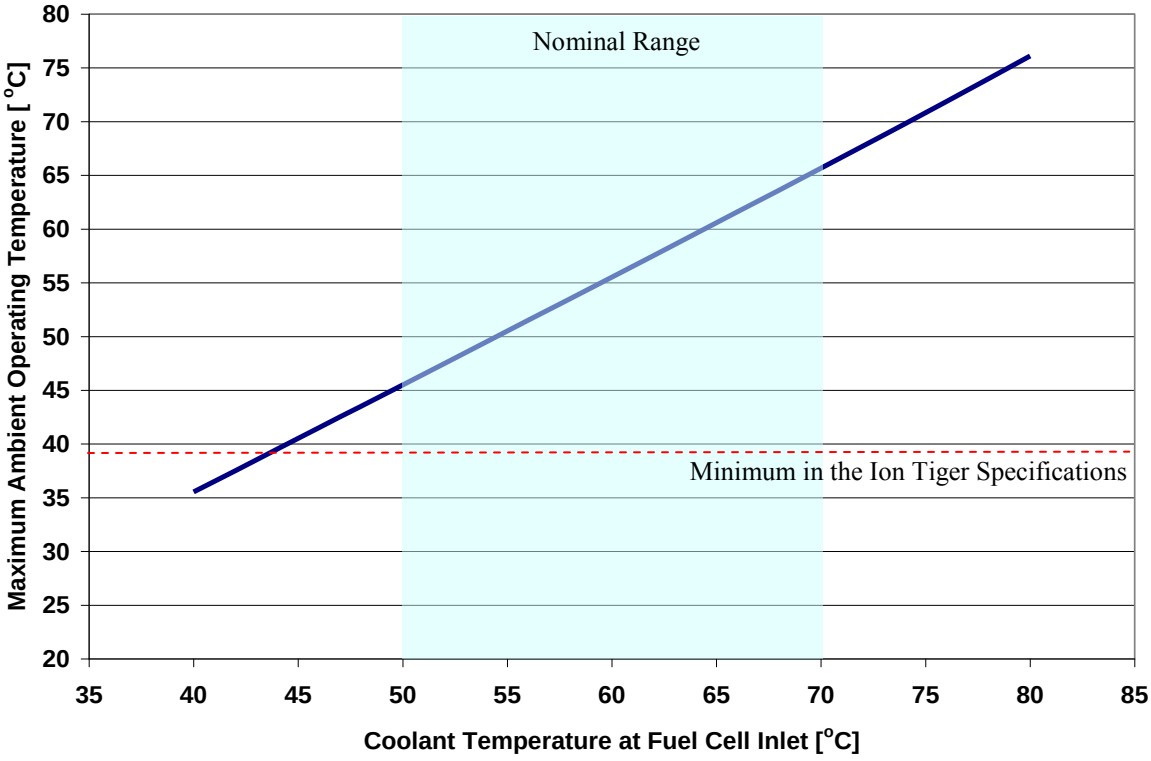

Figure 31. Variation in the maximum ambient operating temperature with changes in the fuel cell stack temperature at the coolant inlet. All other parameters for this simulation can be found in Table XXII.

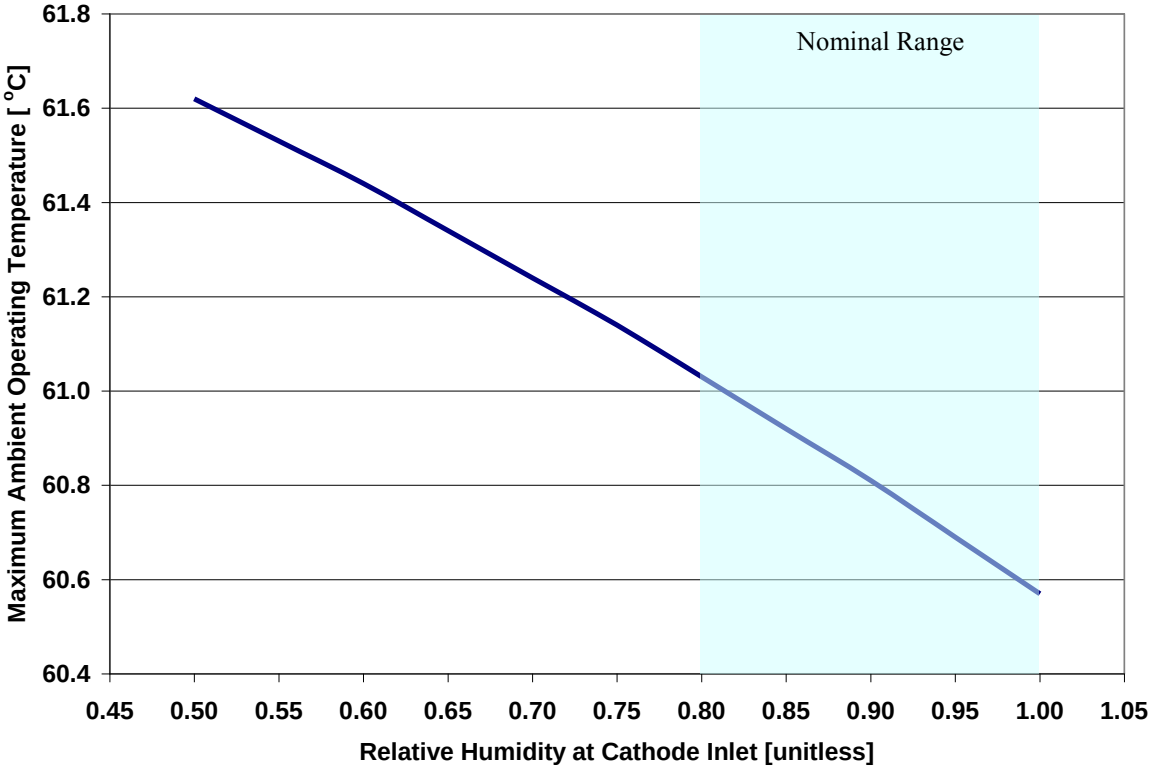

Figure 32. Variation in the maximum ambient operating temperature with changes in the cathode stream relative humidity at the inlet. All other parameters for this simulation can be found in Table XXII.

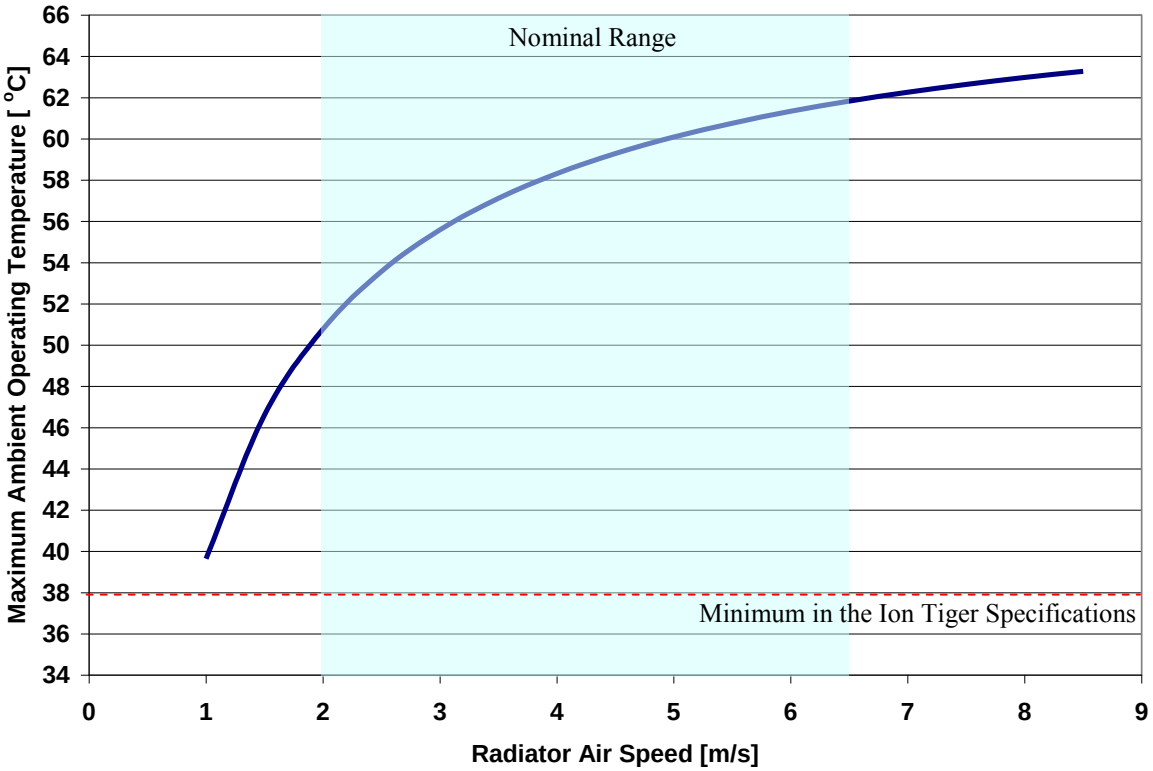

Figure 33. Variation in the maximum ambient operating temperature with changes in the air speed through the radiator. All other parameters for this simulation can be found in Table XXII.

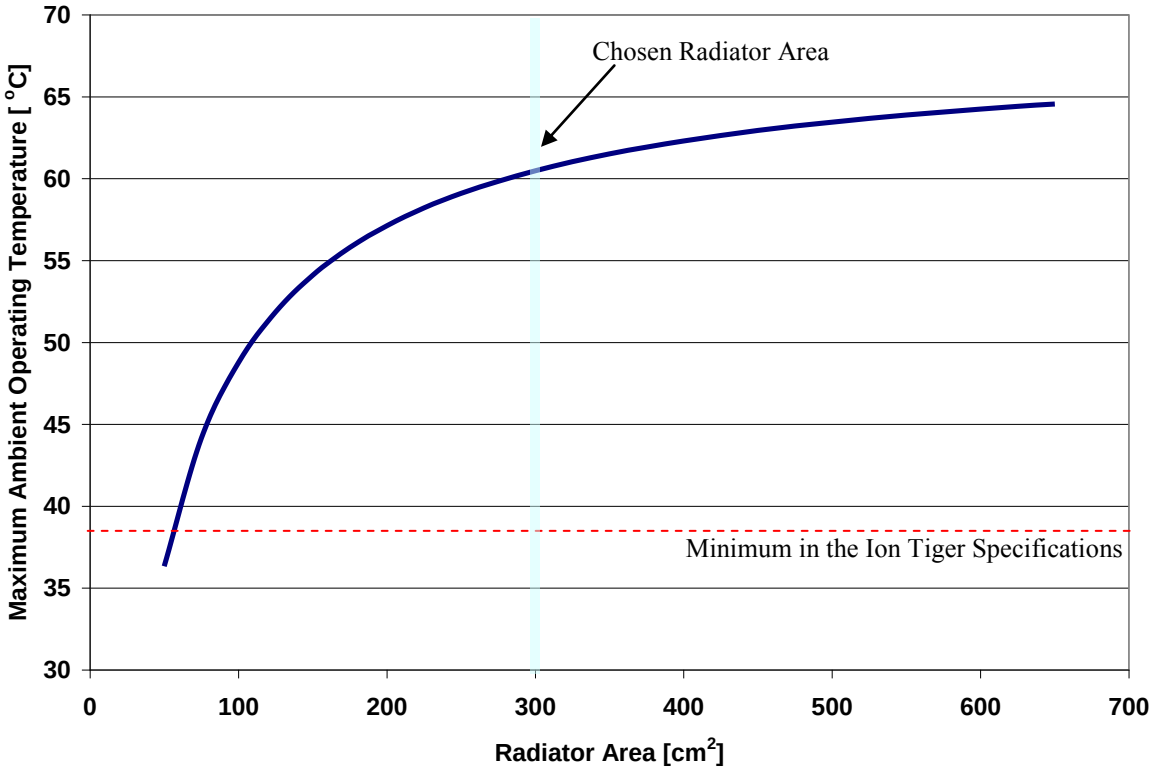

Figure 34. Variation in the maximum ambient operating temperature with changes in the radiator area. All other parameters for this simulation can be found in Table XXII.

Measured Ion Tiger Cooling System Performance

After building the Ion Tiger, the performance of the cooling system was evaluated in a wind tunnel and in flight tests. This section describes some of the measurements of interest and the ways in which they were used to validate the fuel cell energy balance and radiator LMTD models.

A key wind tunnel measurement was the air velocity through the radiator under various operating conditions (see Table XXIII). The lowest air velocity was 2.10 m/s, measured with the radiator cooling fans turned on, the propeller still and no wind in the tunnel. This is effectively the situation when the Ion Tiger is idling on the runway, yet the air velocity is still slightly greater than that used to size the radiator. When the airplane is in flight with the propeller operating, the air velocity through the radiator can be as much as three times higher than that used to size the radiator. This suggests that the safety factor for the radiator when the propulsion motor is at full power and the cooling fans are operating is much larger than originally planned. Repeating calculation #3 in Appendix II with the largest air velocity in Table XXIII indicates that the actual radiator safety factor is ~4. If the fans were removed (as they might be to save weight) then the safety factor would be ~3.2.

TABLE XXIII. Measured air velocity through the Ion Tiger radiator while installed in the NRL wind tunnel. The radiator fans were either off or on (at full power) for these measurements. Tunnel airspeed was varied to simulate the change in aircraft speed with propulsion power.

Propulsion Power [W]	Radiator Fan [on/off]	Tunnel Air Speed [knots]	Air Velocity Thru Radiator [m/s]	Estimated Volumetric Air Flow Rate Through Radiator [ft^3/min]
0	on	0 ± 1	2.10 ± 0.1	135
0	off	25	2.67	172
310	off	25	4.55	293
510	off	29	5.35	344
0	on	25	4.00	257
310	on	25	6.50	418
510	on	29	6.94	447

The fuel cell system reports seven cooling system related parameters to the ground at roughly 1 s intervals. These include the coolant inlet temperature, coolant outlet temperature, air inlet temperature, air outlet temperature, coolant pump voltage, radiator fan control signal, and the bypass valve control signal. Also reported are the fuel cell current, fuel cell voltage and the air blower control signal, all of which are related to the rate of heat production in the fuel cell. A good example of cooling system operation is a test flight which took place on 25 August 2009 in 26 - 28 °C ambient conditions. The cooling system related telemetry from these flights is shown in figures 35 – 37.

Note that in figure 37 the cooling fans were never turned on and the bypass valve directed at most only ~40% of the coolant through the radiator, even when the fuel cell system operated at full power continuously for more than 10 minutes from 17,000 – 20,000 s. Even considering the moderate ambient temperature, these data indicate a substantial safety factor on the radiator area. The coupled fuel cell/radiator model used for the design sensitivity analysis also predicted a substantial safety factor for the conditions of the 25 August 2009 test flight. For the detailed model validation, refer to Appendix II.

The maximum ambient operating temperature for the Ion Tiger with the present radiator and fan assembly was estimated from the data in Table XXIII and figures 35 – 37. The results are shown in Table XXIV. Note that all of the maximum ambient operating temperatures in Table XXIV are greater that the 38 °C minimum specification, so the Ion Tiger cooling system as presently designed should be more than adequate in hot environments.

TABLE XXIV. Predicted maximum ambient operating temperature for the Ion Tiger with the present 304 cm^2 radiator in three scenarios, using the measured cooling system performance data. Rows which vary from one case to another are shaded.

Parameter	Worst Case Scenario	Likely Full Power Scenario	Likely Cruise Power Scenario
Fuel cell heat rejection rate	800 W	800 W	400 W
Fuel cell coolant inlet temperature	55 °C	70 °C	70 °C
Cathode inlet relative humidity	1.0	1.0	1.0
Cathode volumetric flow rate	30 L/min	30 L/min	30 L/min
Coolant flow rate	2 L/min	2 L/min	2 L/min
Air velocity through radiator	6.9	6.9	6.5
Maximum ambient operating temperature	47 °C	55 °C	56 °C

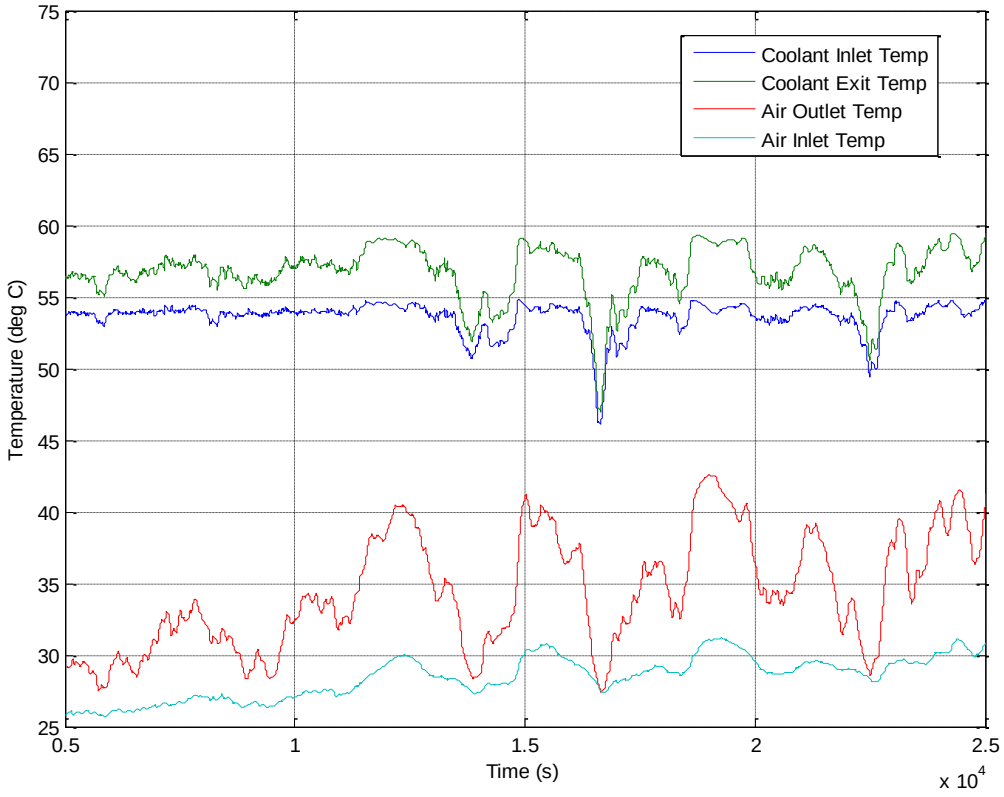

Figure 35. Coolant inlet, coolant outlet, air inlet and air outlet temperatures during a portion of the 25 August 2009 test flight.

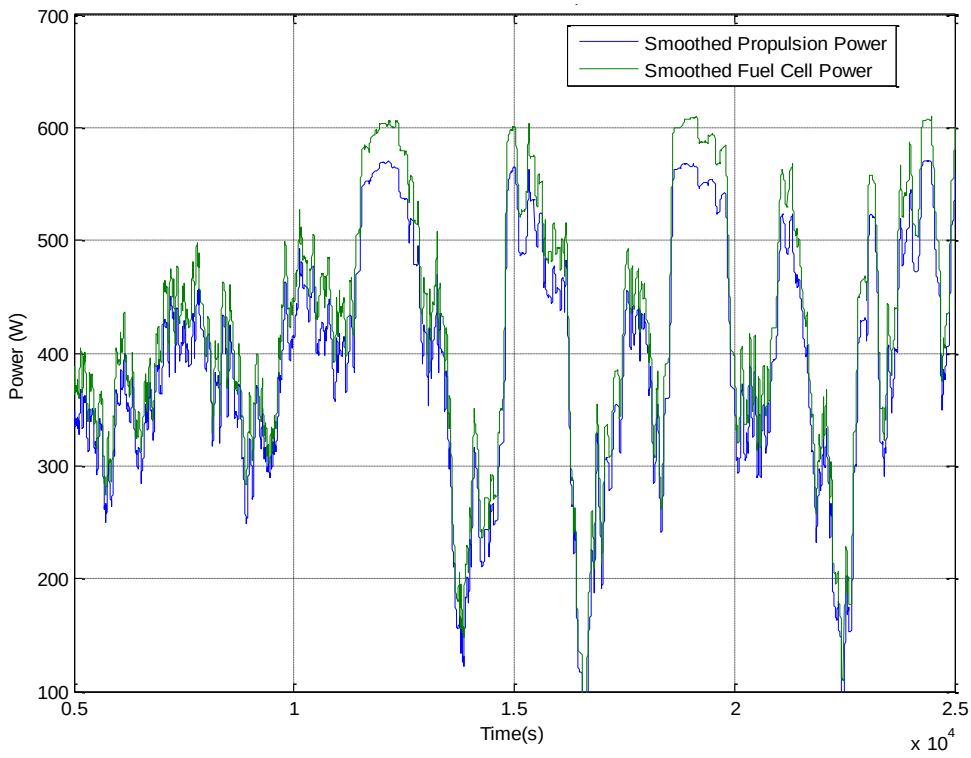

Figure 36. Fuel cell power production and propulsion power consumption during a portion of the 25 August 2009 test flight.

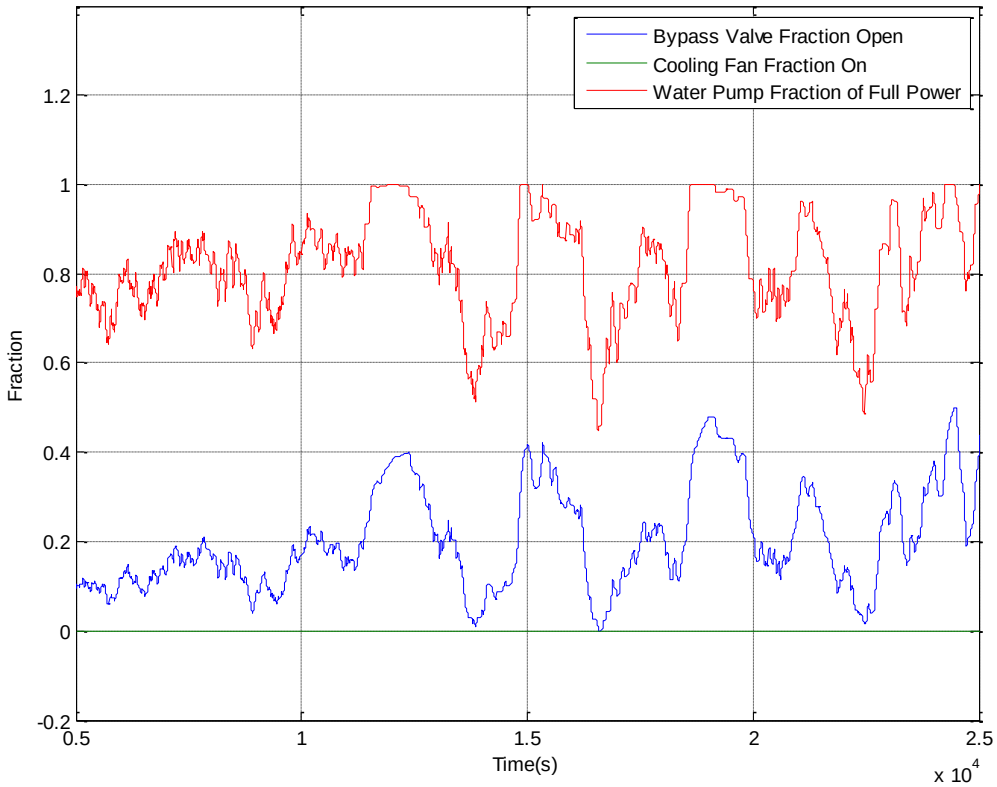

Figure 37. Bypass valve fraction open to radiator, cooling fan fraction of full power and water pump fraction of full power during a portion of the 25 August 2009 test flight.

Conclusions and Recommendations

Rejecting heat with a small temperature gradient is always an engineering challenge, but the difficulty is exacerbated in small aircraft where the heat exchanger mass is severely restricted. All PEMFC powered aircraft must overcome this challenge to be successful, and a solution has been identified for the Ion Tiger. The tools used to develop this solution (test methods and models) are applicable to both larger and smaller PEMFC powered aircraft. The coupled stack/radiator model is applicable to PEMFC systems using a CHE for heat rejection, and could easily be adapted to different radiator and stack sizes, radiator geometries, and humidification methods. Pressurized cathode and recirculating anode PEMFCs could also be treated with minor changes to the model.

The overall heat transfer coefficients of the surface radiators were impractically low; the radiators were too heavy and would have required more area than was available on the aircraft fuselage. All of the single channel radiators had coolant side pressure drops that were far too large for the Ion Tiger fuel cell coolant pumps to overcome at the required flow rates.

Of the radiators examined in this study, CHEs provided the best performance and the most reasonable design space. The tube and louvered fin geometry of radiators #7 and #8 packed a large fin surface area into a small device, saving considerable water weight in tubes and manifolds. The air flow rates required to cool the Ion Tiger with the CHEs were small, reducing fan power consumption to the point where it was worth paying the parasitic fan power penalty in order to use the lightweight radiator. The multiple parallel coolant flow paths in the CHEs yielded low coolant side pressure drop at the required flow rates. Internal tube and fin CHEs are recommended for future PEMFC powered aircraft in the Ion Tiger power range (550 W propulsion) and for larger aircraft. For smaller aircraft there should be a size at which surface radiators become viable due to the greater fuselage surface area/volume ratio, but the size at which that becomes true was not identified in this study.

The models were an essential part of the radiator selection and sizing process. The stack energy balance model predicted the rate of heat rejection, and the radiator models were used to predict radiator performance. With the rate of heat rejection and radiator performance known, the area and mass of each radiator type required by the Ion Tiger could be determined and then compared to select the lightest option. The surface radiator model was also important in that it showed which area (channel or total aluminum plate) to use when computing overall heat transfer coefficients from the wind tunnel measurements.

The stack energy balance model was validated using flight test data, which showed that it accurately predicted the rate of heat rejection to the coolant loop. The radiator models were validated by both experiments and flight test data; the surface radiator and CHE models accurately predicted radiator performance given the air flow rates, water flow rates and temperatures expected in the airplane.

In addition to sizing a radiator for Ion Tiger, the combined stack/radiator model was used to guide future development by identifying trends. It indicated a strong relationship between humidifier effectiveness and radiator size; a more effective humidifier raises the cathode inlet relative humidity, which increases the latent and total heat load. Conversely, raising the fuel cell operating temperature increased the rate of product water evaporation and reduced the latent heat load on the radiator, up to the point at which all of the exhaust water evaporated (~70 °C). Varying the liquid/vapor balance in the fuel cell by operating the fuel cell at the limits of its temperature range caused a change in the required radiator area and mass of over 2X. Thus one of the best ways to reduce the power system mass and improve performance is to run the fuel cell at higher temperatures, which not only reduces radiator size by rejecting more heat through he cathode exhaust, but also makes the radiator more efficient due to the larger radiator – air temperature difference. These effects were observed in the Ion Tiger when the stack temperature was increased by 10 °C. The margin of improvement diminishes with increasing fuel cell temperature, so one must carefully balance the weight penalty associated with operating at higher temperatures (often a larger humidifier) against the potential reduction in cooling system weight (a smaller radiator).

In summary:

- The Ion Tiger cooling system as presently designed has a safety factor of ~4 with respect to the ambient operating temperature specification.
- Internal compact heat exchangers are the lightest and lowest coolant pressure drop option for heat rejection by fuel cell powered aircraft of ~550 W or greater.
- The fuel cell operating temperature should be chosen such that all water in the cathode exhaust is vapor to minimize the required radiator area.
- The models used for this study can be applied (with minor modifications) to the design and sizing of cooling systems for other PEMFC powered vehicles.

The authors would like to thank the Office of Naval Research for funding this work under the Ion Tiger program. We would also like to thank Ian Peek (Naval Surface Warfare Center, Carderock Division) and Drew Rodgers (ITT AES) for their help gathering the experimental data, Nick Lauder (Protonex Technology Corporation) for conversations regarding the fuel cell thermal model and Michael Vick (Naval Research Laboratory) for reviewing the heat transfer calculations.

References

1. Bradley, T. H., Moffitt, B. A., Fuller, T. F., Mavris, D., Parekh, D. E. "Design Studies for Hydrogen Fuel Cell Powered Unmanned Aerial Vehicles", AIAA Paper 2008-6413, Aug. 2003.

2. Kays, William, Michael Crawford and Bernard Weigand, *Convection Heat and Mass Transfer*, 4th Ed., McGraw-Hill, New York, 2005.

3. Incropera, Frank P. and David P. DeWitt, *Fundamentals of Heat and Mass Transfer*, 4th Ed., John Wiley & Sons, New York, 1996.

4. Larminie, James and Andrew Dicks, *Fuel Cell Systems Explained*, 2nd Ed., John Wiley & Sons, New York, 2003.

5. Moran, Michael J. and Howard N. Shapiro, *Fundamentals of Engineering Thermodynamics*, 3rd Ed., John Wiley & Sons, New York, 1995.

Appendix I: Combined Fuel Cell Stack Energy Balance and Radiator Model Code

The following fuel cell stack thermal model code was written for the Engineering Equation Solver (EES) environment. Comma separated lists in parentheses are calls to EES thermophysical functions. Variables appearing in the code are explained in Table I-I.

TABLE I-I. Variables appearing in the fuel cell stack thermal model code.

Variable	Meaning	Unit
P_stack	Gross FC stack electrical output	W
I_stack	FC current	A
V_stack	FC stack voltage	V
N_cells	Number of cells in series in the FCs stack	none
fuel_utilization	Fraction of fuel flow into the FC which is consumed in the reaction	none
T_ambient	Ambient air temperature	°C
P_ambient	Ambient air pressure	kPa
RH_ambient	Ambient air relative humidity	none
T_fc_coolant_in	Temperature of coolant at the stack inlet	°C
T_fc_coolant_out	Temperature of coolant at the stack outlet	°C
Bypass	Fraction of total bypass valve servo travel	none
Coolant_pump_power_fraction	Voltage to the coolant pump as a fraction of the maximum	none
V_dot_coolant	Volumetric flow rate of coolant through the FC stack	m^3/s
RH_cathode_in	Relative humidity of air exiting the humidifier and entering the FC cathode	
V_dot_humidifier_in	Volumetric flow rate of humidified air into the cathode	m^3/s
T_cathode_in	Temperature of air flowing into the FC cathode	°C
T_cathode_out	Temperature of air flowing out of the FC cathode	°C
T_anode_in	Temperature of H_2 flowing into the FC anode	°C
T_anode_out	Temperature of H_2 flowing out of the FC anode	°C
P_anode_gauge_in	Gauge pressure of H_2 at the FC anode inlet	psi
P_anode_gauge_out	Gauge pressure of H_2 at the FC anode outlet	psi
P_cathode_gauge_in	Gauge pressure of air at the cathode inlet	psi
P_cathode_gaude_out	Gauge pressure of air at the cathode outlet	psi
P_anode_in	Absolute pressure of H_2 at the anode inlet	kPa
P_anode_out	Absolute pressure of H_2 at the anode outlet	kPa
P_cathode_in	Absolute pressure of air at the cathode inlet	kPa
P_cathode_out	Absolute pressure of air at the cathode outlet	kPa
area_radiator	Area of radiator perpendicular to the direction of air flow	m^2
Q_dot_radiator	Rate of heat rejection from the radiator	W
v_radiator_airflow	Velocity of air flowing through area_radiator	m/s
U_rad	Overall heat transfer coefficient of the radiator	$W/(m^2\ °C)$
T_LMTD	Log mean temperature difference of the radiator and ambient air	°C
n_dot_radiator_air	Molar flow rate of ambient air through the radiator	mol/s
F	Faraday's constant	mol/C
H2O_molar_mass	Molar mass of water	g/mol
air_dry_molar_mass	Mean molar mass of dry air	g/mol
h_formation_H2O_gas	Enthalpy of formation for water vapor	J
h_formation_H2O_liq	Enthalpy of formation for liquid water	J
h_vaporization_H2O	Heat of vaporization of water	J
n_dot_O2_consumed	Rate of O_2 consumption by the FC	mol/s
n_dot_H2O_produced	Rate of water production by the FC	mol/s
n_dot_H2_consumed	Rate of H_2 consumption by the FC	mol/s
n_dot_coolant	Molar flow rate of coolant through the FC stack	mol/s
rho_ambient_air	Density of ambient air	kg/m^3
humidrat_ambient_air_mol	Humidity ratio of ambient air	none
n_dot_ambient_air_in	Molar flow rate of ambient air into the humidifier	mol/s
n_dot_ambient_air_H2O_in	Molar flow rate of water vapor carried into the humidifier by the ambient air	mol/s
n_dot_ambient_air_dry	Molar flow rate of ambient air into the humidifier, without any water vapor	mol/s
humidrat_cathode_air_in_mol	Humidity ratio of air exiting the humidifier and entering the FC cathode	
n_dot_cathode_in_H2O	Molar flow rate of water vapor carried into the FC by the cathode inlet flow	mol/s
n_dot_cathode_in	Total molar flow rate into the FC cathode	mol/s
n_dot_cathode_out_dryair	Molar flow rate of dry air out of the FC cathode	mol/s
n_dot_cathode_out_H2O	Molar flow rate of water (both vapor and liquid) from the FC cathode outlet	mol/s
n_dot_cathode_out_H2O_vap	Molar flow rate of water vapor from the FC cathode outlet	mol/s
n_dot_cathode_out_H2O_liq	Molar flow rate of liquid water from the FC cathode outlet	mol/s
humidrat_cathode_out_mass_pre	Humidity ratio of cathode outlet flow, mass basis, before adjusting to account for the maximum ratio being 1.0	none

RH_cathode_out_pre	Relative humidity of cathode outlet flow before adjusting to account for the maximum ratio being 1.0	none
humidrat_cathode_out_mass_act	Actual humidity ratio of the cathode outlet flow, mass basis	none
RH_cathode_out_actua	Actual relative humidity of the cathode outlet flow	none
quality_cathode_out	Quality of the cathode outlet flow (fraction of the water which is vapor)	none
n_dot_anode_in	Molar flow rate of H_2 into the FC anode	mol/s
n_dot_anode_out	Molar flow rate of H_2 out of the FC anode	mol/s
h_dot_anode_in	Rate of enthalpy flow into the FC anode	W
h_dot_anode_out	Rate of enthalpy flow out of the FC anode	W
h_dot_cathode_in	Rate of enthalpy flow into the FC cathode	W
h_dot_cathode_out	Rate of enthalpy flow out of the FC cathode	W
h_dot_reaction	Rate of enthalpy generation by the reaction	W
eta_LHV	FC thermal efficiency based on the lower heating value of H_2	none
eta_HHV	FC thermal efficiency based on the higher heating value of H_2	none
deltaT_coolant_thru_radiator	Change in coolant temperature as it flows through the radiator	°C
T_coolant_ave_inside_radiator	Mean temperature of coolant inside the radiator	°C
deltaT_air_thru_radiator	Change in air temperature as it flows through the radiator	°C
T_air_ave_inside_radiator	Mean temperature of coolant inside the radiator	°C
rho_radiator	Area density of the radiator	kg/m^2
mass_radiator	Mass of the radiator	kg

```
"Functions"

FUNCTION
cathode_vapor_flow(RH_cathode_out_pre,n_dot_cathode_out_H2O,T_cathode_out,P_cathode_out,air_dry_molar_mass,H2O_molar_mass,n_dot_cathode_out_d
ryair)
{This funtion determines the water vapor molar flow rate at the cathode exit, with the IF-THEN handling saturated and unsaturated conditions}
IF (RH_cathode_out_pre < 1) THEN
        cathode_vapor_flow = n_dot_cathode_out_H2O                      {mol/s}
        ELSE
        saturated_humrat_mol = HumRat(AirH2O,T=T_cathode_out, r=1, P=P_cathode_out) * air_dry_molar_mass/H2O_molar_mass
        cathode_vapor_flow = saturated_humrat_mol * n_dot_cathode_out_dryair     {mol/s}
ENDIF
END

"-------------------------------------------------------------------------------------------------------------------------------------------
Setup System to be Modeled
-------------------------------------------------------------------------------------------------------------------------------------------"

"Fuel Cell Stack  Characteristics"
P_stack = 600                           {W}
I_stack = P_stack/V_stack               {A}
V_stack = 4.859E-8 * I_stack^6 - 5.74E-6* I_stack^5 + 2.794E-4 * I_stack^4 - 7.5724E-3*I_stack^3 + 0.12087*I_stack^2 - 1.3190151*I_stack + 33.20411  {V}
N_cells = 36
fuel_utilization = 0.99

"Ambient Conditions"
T_ambient = 30.8                                                        {deg C}
P_ambient = 101                                                         {kPa}
RH_ambient = 0.40                                                       {ratio}

"Coolant Flow Parameters"
T_fc_coolant_in = 54.3                                                  {deg C}
{T_fc_coolant_out = 58.9}                                               {deg C}
Bypass = 0.43                                                           {fraction open to radiator}
Coolant_pump_power_fraction = 1.00                                      {fraction of coolant pump full power}
V_dot_coolant = Coolant_pump_power_fraction * 2.0 / (1000 * 60)         {m^3/s}
T_fc_coolant_in = (1-Bypass) * T_radiator_coolant_out + Bypass *  T_fc_coolant_out      {deg C}

"Cathode and Anode Flow Parameters"
RH_cathode_in = 1
V_dot_humidifier_in = 30/(1000 * 60)                {m^3/s}
T_cathode_in = 0.5 * (T_ambient + T_cathode_out)    {deg C}
T_cathode_out = T_fc_coolant_out                    {deg C}
T_anode_in = T_ambient                              {deg C}
T_anode_out = T_fc_coolant_out                      {deg C}
P_anode_gauge_in = 16                               {psi}
P_cathode_gauge_in = 0.5                            {psi}
P_anode_gauge_out = 16                              {psi}
P_cathode_gauge_out = 0                             {psi}

P_anode_in = P_ambient + P_anode_gauge_in * 6.8947              {kPa}
P_cathode_in = P_ambient + P_cathode_gauge_in * 6.8947          {kPa}
P_anode_out = P_ambient + P_anode_gauge_out * 6.8947            {kPa}
P_cathode_out = P_ambient + P_cathode_gauge_out * 6.8947        {kPa}
```

```
"Radiator Parameters"
area_radiator = 0.0304                                          {m^2}
area_radiator = Q_dot_radiator/(U_rad * T_LMTD)                 {m^2}
v_radiator_airflow = 3                                          {m/s}
U_rad = 1269*v_radiator_airflow + 99.9                          {W/(m^2*K)}
n_dot_radiator_air = v_radiator_airflow * area_radiator * Density(Air_ha, T=T_ambient, P=P_ambient) * 1000          {mol/s}

"Constants and Thermophysical Data"
F = 96485                                                                                             {C/mol}
H2O_molar_mass = 18                                                                                   {g/mol}
air_dry_molar_mass = 28.964                                                                           {g/mol}
h_formation_H2O_gas = 228590 - (T_coolant_ave_inside_radiator  + 273.15) * (188.72 - 130.57 - 0.5 * 205.03)   {J/mol} {Moran and Shapiro}
h_formation_H2O_liq = 285830                                                                          {J/mol} {Moran and Shapiro}
h_vaporization_H2O = 40650                                                                            {J/mol} {Wikipedia}

"------------------------------------------------------------------------------------------------------------------------------------------------------
Compute Flow Rates and Enthalpies
------------------------------------------------------------------------------------------------------------------------------------------------------"

"Reactant and Product Reaction Rates"
n_dot_O2_consumed  =  I_stack * N_cells / (4 * F)               {mol/s}
n_dot_H2O_produced = I_stack* N_cells / (2 * F)                 {mol/s}
n_dot_H2_consumed  = I_stack * N_cells / (2 * F)                {mol/s}

"Calculate the molar flowrates of coolant , air and water vapor into/out of stack"

"Coolant flow rate"
n_dot_coolant = (Density(Water, T= T_fc_coolant_out, P = P_ambient)) *1000* V_dot_coolant                      {mol/s}

"Air at the humidifier inlet"
rho_ambient_air = Density(AirH2O, T = T_ambient, r = RH_ambient, P = P_ambient)*1000                          {mol/m^3}
humidrat_ambient_air_mol = HumRat(AirH2O,T=T_ambient ,r = RH_ambient, P = P_ambient) * air_dry_molar_mass/H2O_molar_mass    {ratio}
n_dot_ambient_air_in = rho_ambient_air * V_dot_humidifier_in                                                   {mol/s}
n_dot_ambient_air_H2O_in = n_dot_ambient_air_in/(1/humidrat_ambient_air_mol + 1)                               {mol/s}
n_dot_ambient_air_dry_in = n_dot_ambient_air_in - n_dot_ambient_air_H2O_in                                     {mol/s}

"Air at the cathode inlet"
humidrat_cathode_air_in_mol = HumRat(AirH2O, T = T_cathode_in, r = RH_cathode_in, P = P_cathode_in) * air_dry_molar_mass/H2O_molar_mass   {ratio}
n_dot_cathode_in_H2O = humidrat_cathode_air_in_mol * n_dot_ambient_air_dry_in                                  {mol/s}
n_dot_cathode_in = n_dot_cathode_in_H2O + n_dot_ambient_air_dry_in                                             {mol/s}

"Air at the cathode outlet"
n_dot_cathode_out_dryair = n_dot_ambient_air_dry_in - n_dot_O2_consumed                                        {mol/s}
n_dot_cathode_out_H2O = n_dot_cathode_in_H2O + n_dot_H2O_produced                                              {mol/s}
n_dot_cathode_out_H2O_vap =
cathode_vapor_flow(RH_cathode_out_pre,n_dot_cathode_out_H2O,T_cathode_out,P_cathode_out,air_dry_molar_mass,H2O_molar_mass,n_dot_cathode_out_d
ryair)
n_dot_cathode_out_H2O_liq = n_dot_cathode_out_H2O - n_dot_cathode_out_H2O_vap                                  {mol/s}

humidrat_cathode_out_mass_pre =  n_dot_cathode_out_H2O/n_dot_cathode_out_dryair * H2O_molar_mass/air_dry_molar_mass          {ratio}
RH_cathode_out_pre = RelHum(AirH2O,T=T_cathode_out, w=humidrat_cathode_out_mass_pre, P=P_cathode_out)                         {ratio}
humidrat_cathode_out_mass_act = n_dot_cathode_out_H2O_vap/n_dot_cathode_out_dryair * H2O_molar_mass/air_dry_molar_mass       {ratio}
RH_cathode_out_actual = RelHum(AirH2O,T=T_cathode_out, w= humidrat_cathode_out_mass_act, P = P_cathode_out)                  {ratio}
quality_cathode_out = n_dot_cathode_out_H2O_vap/n_dot_cathode_out_H2O                                                         {ratio}

"Hydrogen at the anode inlet"
n_dot_anode_in = n_dot_H2_consumed + n_dot_anode_out                                                           {mol/s}

"Hydrogen at the anode outlet"
n_dot_anode_out = n_dot_anode_in * (1 - fuel_utilization)                                                      {mol/s}

"Compute the Enthalpies of the Streams"

h_dot_anode_in     = (Enthalpy(Hydrogen,T=T_anode_in, P=P_anode_in) - Enthalpy(Hydrogen,T=25, P=101)) * n_dot_anode_in          {W}
h_dot_anode_out  = (Enthalpy(Hydrogen,T=T_anode_out, P=P_anode_out) - Enthalpy(Hydrogen,T=25, P=101)) * n_dot_anode_out      {W}

h_dot_cathode_in    = (Enthalpy(AirH2O, T = T_cathode_in, r = RH_cathode_in, P = P_cathode_in) - Enthalpy(AirH2O, T = 25, r = 0.5, P = 101)) *
n_dot_ambient_air_dry_in                                                                                       {W}
h_dot_cathode_out = (Enthalpy(AirH2O, T = T_cathode_out, w= humidrat_cathode_out_mass_act, P = P_cathode_out) - Enthalpy(AirH2O, T = 25, r = 1, P =
101))* n_dot_cathode_out_dryair - h_vaporization_H2O * n_dot_cathode_out_H2O_liq

h_dot_reaction = h_formation_H2O_gas * n_dot_H2O_produced                                                      {W}

"------------------------------------------------------------------------------------------------------------------------------------------------------
Solve Stack Energy Balance
------------------------------------------------------------------------------------------------------------------------------------------------------"

h_dot_reaction + h_dot_cathode_in + h_dot_anode_in = Q_dot_radiator + P_stack + h_dot_cathode_out +  h_dot_anode_out    {W}
Q_dot_cathode = h_dot_cathode_out - h_dot_cathode_in                                 {W}
Q_dot_anode = h_dot_anode_out - h_dot_anode_in                                       {W}
Q_dot_thermal = Q_dot_radiator + Q_dot_cathode + Q_dot_anode                         {W}
eta_LHV = P_stack/(h_formation_H2O_gas * n_dot_H2O_produced)                         {unitless}
eta_HHV = P_stack/(h_formation_H2O_liq  * n_dot_H2O_produced)                        {unitless}
```

```
"-----------------------------------------------------------------------------------------------------------------------------------------------------------
Solve Radiator Energy Balances
-----------------------------------------------------------------------------------------------------------------------------------------------------------"

"Calculate radiator and coolant related temperatures"
deltaT_coolant_thru_radiator = Q_dot_radiator/(n_dot_coolant * Cp(Water, T = T_coolant_ave_inside_radiator, P = P_ambient)) {deg C}
deltaT_coolant_thru_radiator = T_fc_coolant_out - T_radiator_coolant_out                                                    {deg C}
T_coolant_ave_inside_radiator = 0.5 * (T_radiator_coolant_out + T_fc_coolant_out)                                           {deg C}

"Calculate radiator and air related temperatures"
deltaT_air_thru_radiator = Q_dot_radiator/(n_dot_radiator_air * Cp(Air_ha, T =T_air_ave_inside_radiator, P = P_ambient))     {deg C}
deltaT_air_thru_radiator = T_air_radiator_outlet - T_ambient                                                                {deg C}
T_air_ave_inside_radiator = 0.5*(T_ambient + T_air_radiator_outlet)                                                         {deg C}

"Calculate radiator and air related temperatures"
T_LMTD= ((T_fc_coolant_out  - T_air_radiator_outlet) - (T_radiator_coolant_out - T_ambient))/ln((T_fc_coolant_out  -
T_air_radiator_outlet)/(T_radiator_coolant_out - T_ambient))

"-----------------------------------------------------------------------------------------------------------------------------------------------------------
Compute Radiator Properties
-----------------------------------------------------------------------------------------------------------------------------------------------------------"
rho_radiator = 19.7                                 {kg/m^2}
mass_radiator = area_radiator * rho_radiator        {kg}
```

Appendix II: Fuel Cell Stack Energy Balance Model Validation Based on a Test Flight

The fuel cell stack energy balance model was validated by comparing its predictions to flight data from 25 August 2009. During this flight the Ion Tiger spent ~20 min operating at full power, which provided a good approximation to steady state for the comparison. The measured fuel cell system characteristics for the ~20 min period were used as parameters in the model, and then the model was used to predict the coolant outlet temperature from the fuel cell. Predicting the outlet coolant temperature indicates whether or not the model is correctly computing the rate of heat production by the fuel cell and the effects of the latent load imposed by the cathode and anode streams.

Table II-I lists the parameters from the flight which were used in the model. Figures II-1 to II-3 show the measured data used for the validation process. The measured fuel cell coolant outlet temperature was 58.9 °C and the predicted coolant outlet temperature was 59.9 °C; the error in the coolant temperature change through the stack is 15%. There are two likely sources of error which would produce an overestimate of the coolant outlet temperature as seen here. First, there is heat loss from the fuel cell stack to air inside the fuselage due to convection, which the model assumes is zero. Second, the model assumes that the bypass valve divides the coolant flows by exactly the fraction of total valve travel, which overestimates the rate of coolant flow through the radiator. If the bypass fraction is adjusted from 0.43 to 0.35, which is easily within the range of error associated with the bypass valve controls, the model and measurements agree. If the coolant flowrate as a function of bypass fraction were measured to create an empirical relation and included in the model, the error would be much smaller. Note that the error in coolant outlet temperature has little effect on the radiator sizing calculations, because the total heat rejection rate matters more than the temperature of the coolant.

TABLE II-I. Measured parameters from the flight data which were used in the model.

Measured Parameter Name	Measured Value Used In Model
Fuel cell stack gross electrical power output	600 W
Ambient temperature	30.8 °C
Cathode inlet relative humidity	1.0
Cathode volumetric flow rate	30 L/min
Coolant flow rate	2.0 L/min
Bypass fraction	0.43
Fuel utilization	0.99
Coolant temperature at the fuel cell inlet	54.3 °C

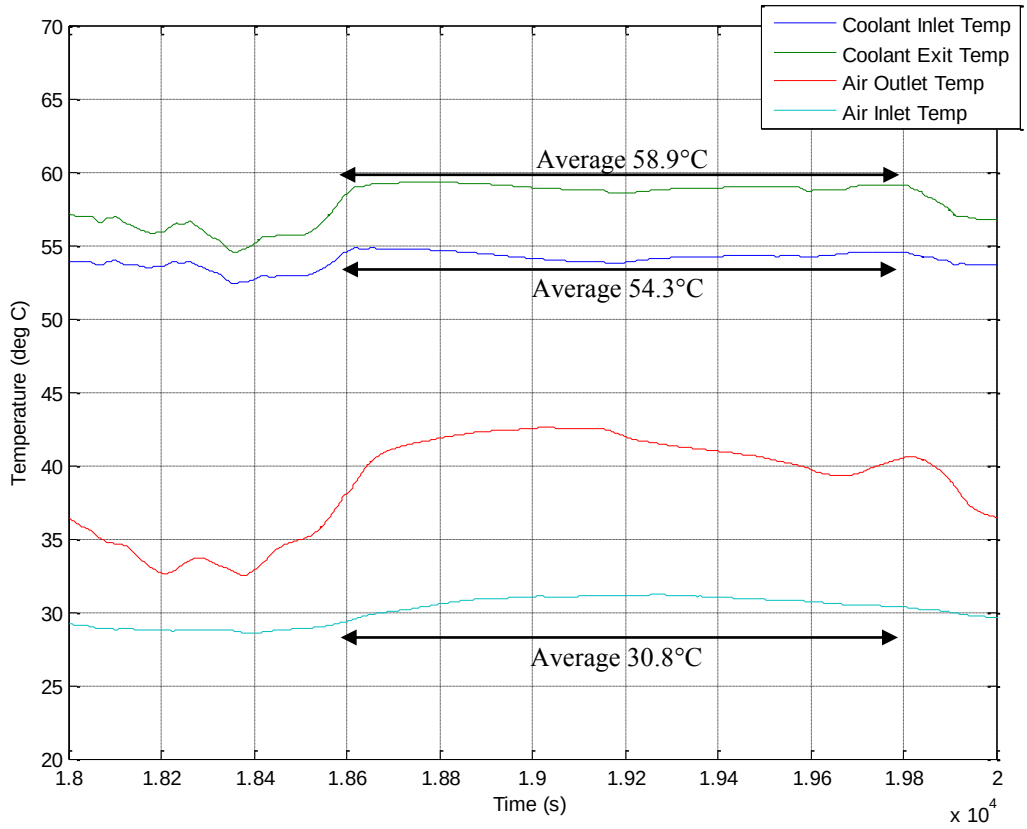

Figure II-1. Coolant inlet, coolant outlet, air inlet and air outlet temperatures during the ~20 minute portion of the 25 August 2009 test flight used to validate the stack thermal model.

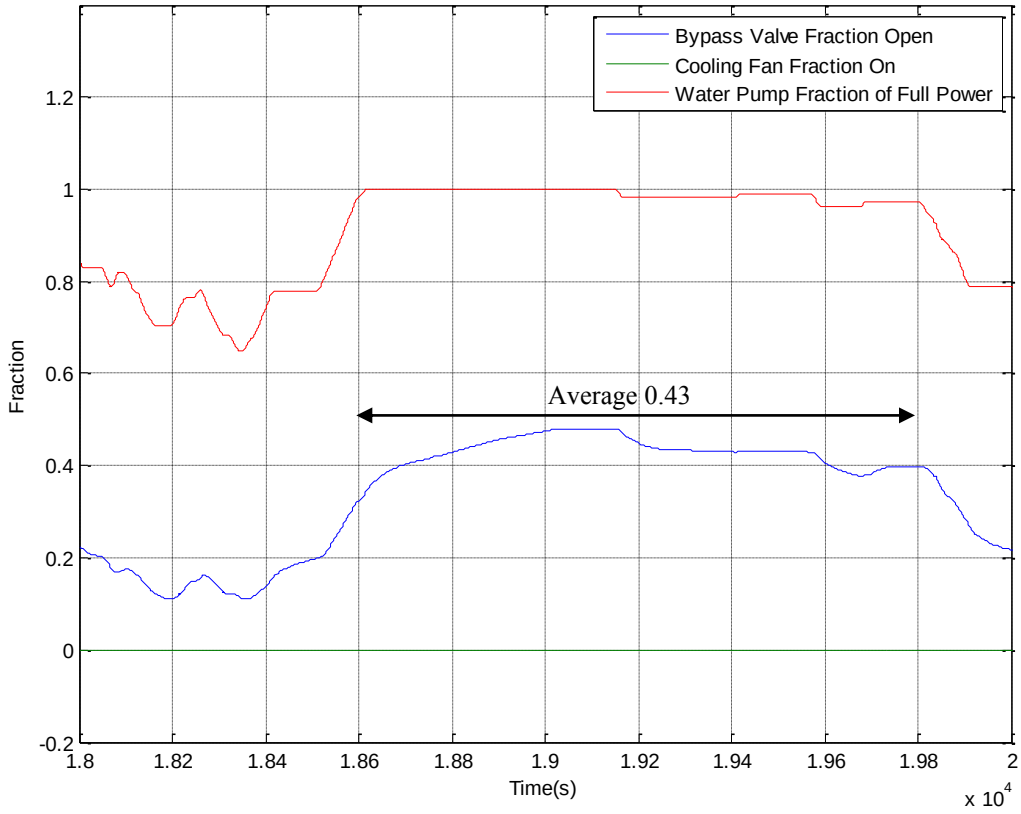

Figure II-2. Bypass valve fraction open, water pump fraction of full power and cooling fan fraction on during the ~20 minute portion of the 25 August 2009 test flight used to validate the stack thermal model.

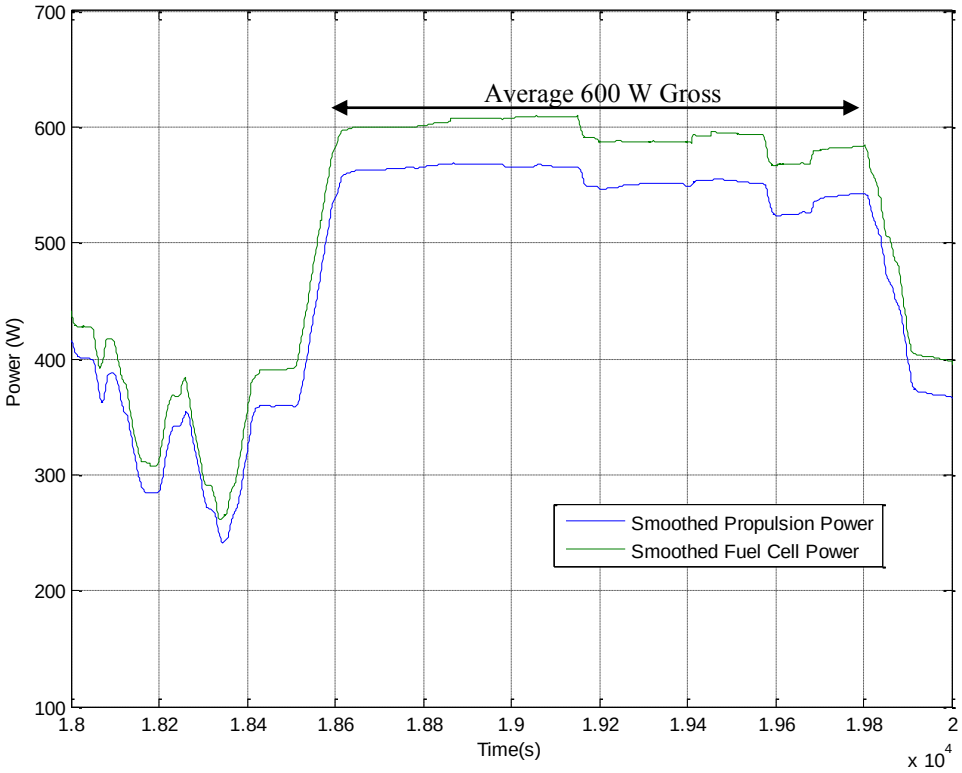

Figure II-3. Fuel cell power output and propulsion power consumption during the ~20 minute portion of the 25 August 2009 test flight used to validate the stack thermal model.

Appendix III: Radiator Sizing Details

Calculation #1: Area and mass of radiator #3 scaled to the Ion Tiger heat load in the worst case ambient air temperature.

Waste heat production rate from the fuel cell stack thermal model: Q_{rad} = 800 W_t
Worst case fuel cell coolant inlet temperature: $T_{coolant,out}$ = 55 °C
Worst case ambient air temperature: $T_{air,in}$ = 38 °C
Best U_{rad} from Table V (one serpentine channel spaced closely) @ 27 knots airspeed: U_{rad} = 50 W/(m^2 °C)
Density of water at 55 °C, 1ATM: ρ_{water} = 0.980 g/cm^3
Density of aluminum at 55 °C, 1ATM: ρ_{Al} = 2.695 g/cm^3
Width of aluminum side of channel: $W_{channel}$ = 0.35 in (0.889 cm)
Aluminum sheet thickness: D_{Al} = 0.005 in (0.0127 cm)

The change in coolant temperature to reject 800 W is calculated using equation 4:

$$\Delta T_{coolant} = \frac{Q_{rad}}{\dot{m}_{coolant} c_{p,water}} = \frac{800\ \text{W}}{(0.03266\ \text{kg/sec})(4183\ \text{J/(kg}\ ^\circ\text{C)})} = 5.86\ ^\circ\text{C}$$

Therefore the average temperature difference between the air and radiator is:

$$\Delta T_{air-radiator} = \frac{1}{2}(55\ ^\circ\text{C} + (55 + 5.86)\ ^\circ\text{C}) - 38\ ^\circ\text{C} = 19.9\ ^\circ\text{C}$$

The minimum aluminum surface area is:

$$A_{norm} = \frac{\dot{Q}_{rad}}{U_{rad}\Delta T_{air-rad}} = \frac{800\text{W}}{\left(50\ \frac{\text{W}}{\text{m}^2\ ^\circ\text{C}}\right)(19.9\ ^\circ\text{C})} = 8040\ \text{cm}^2$$

This area does not include the manifolds. The tested radiator panel had an area of 1393 cm^2, so 8040 cm^2 /1393 cm^2 = 5.8 radiators such as the one evaluated in the wind tunnel would be required to cool the Ion Tiger. Each radiator has a total channel length of 403 cm, so the total channel length would be:

$$L_{channel} = (6.75)(403\text{cm}) = 2325\ \text{cm}$$

The cross section area of the channel (assuming the same profile as the test radiator) is:

$$A_{Xchannel} = \tfrac{1}{2}(0.889\ \text{cm})(0.766\ \text{cm}) = 0.340\ \text{cm}^2$$

The total volume of channel required is:

$$V_{channel} = A_{Xchannel} L_{channel} = (0.340\ \text{cm}^2)(2325\ \text{cm}) = 790\ \text{cm}^3$$

The minimum water mass is:

$$m_{water} = V_{channel}\rho_{water} = (790\ \text{cm}^3)\left(0.980\ \frac{\text{g}}{\text{cm}^3}\right) = 744\ \text{g}$$

The volume of aluminum required is:

$$V_{Al} = L_{channel} W_{channel} D_{Al} = (9411\ \text{cm}^2)(0.0127\ \text{cm}) = 102\ \text{cm}^3$$

The minimum aluminum mass is:

$$m_{Al} = V_{Al}\rho_{Al} = \left(102\,\text{cm}^3\right)\left(2.695\,\frac{\text{g}}{\text{cm}^3}\right) = 275\,\text{g}$$

Adding the water and aluminum masses gives a total minimum radiator mass of 1019 g. This does not include the mass of aluminum between channels, nor does it include the added weight of the larger carbon fiber area once it is "rippled" to produce channels in the fuselage.

Calculation #2: Area and mass of radiator #5 if it were scaled for the heat load and air flow rate in the Ion Tiger.

Waste heat production rate from the fuel cell stack thermal model: Q_{rad} = 800 W_t
Worst case air-radiator temperature difference ΔT_{lmtd} = 19.9 °C (see calculation #1)
Worst case ambient air temperature: $T_{air,in}$ = 38 °C
U_{rad} from Table VII @ 27 knots airspeed: U_{rad} = 1478 W/(m^2 °C)
Radiator #5 area density: 2.08 g/cm^2

The radiator area required using equation 5:

$$\frac{800\text{W}}{\left(1478\,\frac{\text{W}}{\text{m}^2\ ^\circ\text{C}}\right)\left(19.9\ ^\circ\text{C}\right)} = 272\text{cm}^2$$

The radiator mass is:

$$\left(272\text{cm}^2\right)\left(2.08\,\frac{\text{g}}{\text{cm}^2}\right) = 566\text{g}$$

This is equivalent to using 272 cm^2/37 cm^2 = 7.4 of the radiator as evaluated in the wind tunnel.

Calculation #3: Area and mass of radiator #8 if it were scaled for the heat load and air flow rate in the Ion Tiger.

Waste heat production rate from the fuel cell stack thermal model: Q_{rad} = 800 W_t
Worst case fuel cell coolant inlet temperature: $T_{coolant,out}$ = 55 °C
Worst case fuel cell coolant outlet temperature: $T_{coolant,in}$ = 60.9 °C
Worst case ambient air temperature: $T_{air,in}$ = 38 °C
Radiator #8 area density: 1.97 g/cm^2
Air velocity through the radiator: 2.0 m/s

To find the radiator area we solve two equations for two unknowns, A_{rad} and $T_{air,out}$:

Equation 4: $$\dot{Q}_{rad} = \rho_{air} v_{air} A_{rad} c_{p,air}\left(T_{air,in} - T_{air,out}\right)$$

Equation 5: $$U_{rad} = \frac{\dot{Q}_{rad}}{A_{rad}\Delta T_{air-radiator}}$$

U_{rad} is computed using the air velocity and equation 18, and the air-radiator temperature difference $\Delta T_{air\text{-}coolant}$ is the log mean temperature difference in equation 8. There are several ways to solve these equations, but since equation 8 is non-linear, the simplest is to divide both by A_{rad} and plot them as functions of $T_{air,out}$. The intersection of the two lines indicates the value of $T_{air,out}$ (see figure AII-1). Using $T_{air,out}$ we can then compute A_{rad}.

$$T_{air,out} = 50.1\ ^\circ\text{C}$$

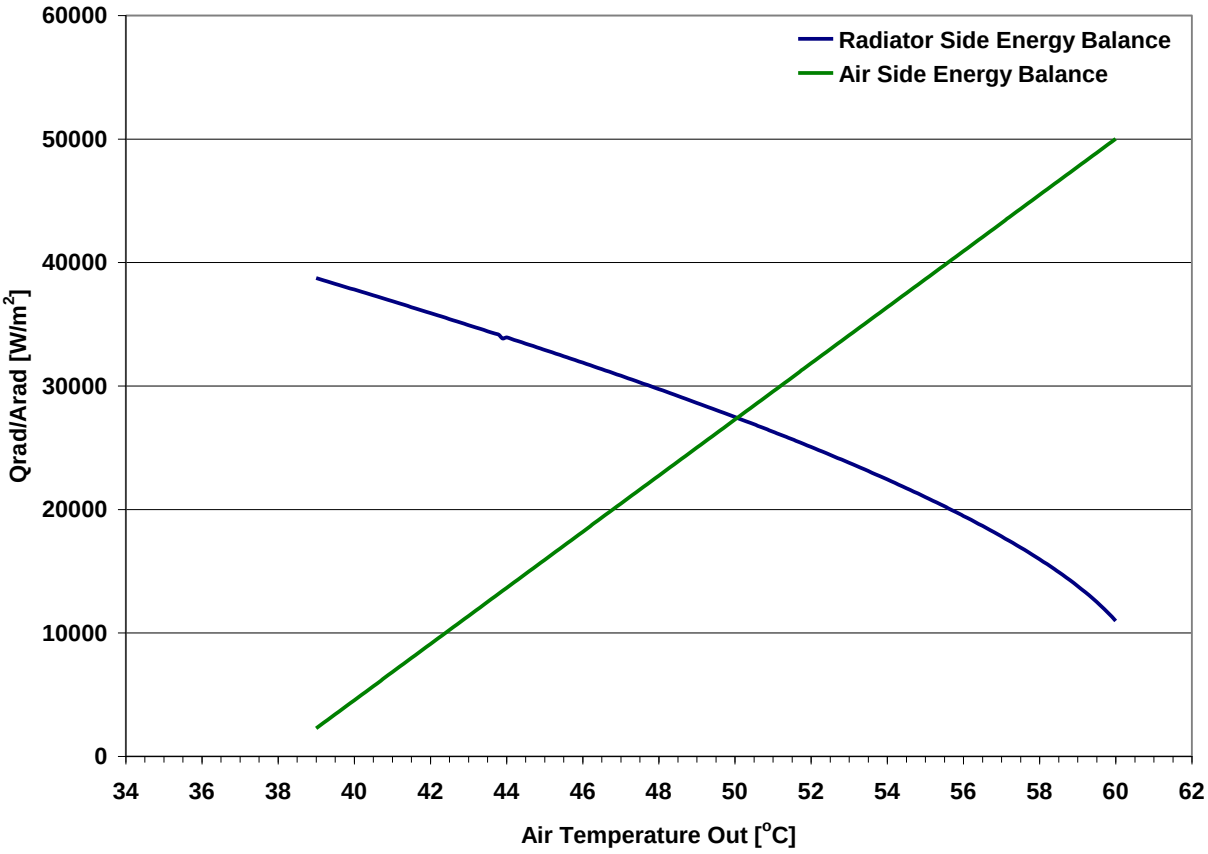

Figure III-1. Plot of radiator heat flux (W/m^2) computed using equation 4 for the air side energy balance and equation 5 for the radiator energy balance. The air outlet temperature is found where the two curves cross.

Solving equation 4 for the radiator area yields:

$$A_{rad} = \frac{\dot{Q}_{rad}}{\rho_{air} v_{air} c_{p,air} \left(T_{air,in} - T_{air,out}\right)} = 246\,\text{cm}^2$$

The radiator mass is:

$$\left(246\text{cm}^2\right)\left(1.97\frac{\text{g}}{\text{cm}^2}\right) = 484\text{g}$$

The air flow rate through the radiator is:

$$\left(2.0\frac{\text{m}}{\text{s}}\right)\left(0.0246\text{m}^2\right)\left(60\frac{\text{s}}{\text{min}}\right)\left(35.31\frac{\text{ft}^3}{\text{m}^3}\right) = 104\frac{\text{ft}^3}{\text{min}}$$

This is equivalent to using 246 cm^2 / 304 cm^2 = 0.8 of radiator #8.